NASA TECHNICAL NOTE

NASA TN D-2366

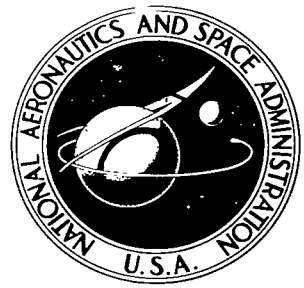

NASA TN D-2366

AN ANALOG STUDY OF A ROTATING-SOLID-ROCKET CONTROL SYSTEM AND ITS APPLICATION TO ATTITUDE CONTROL OF A SPACE-VEHICLE UPPER STAGE

by A. Thomas Young and Jack E. Harris

Langley Research Center
Langley Station, Hampton, Va.

NATIONAL AERONAUTICS AND SPACE ADMINISTRATION • WASHINGTON, D. C. • AUGUST 1964

ERRATA

NASA Technical Note D-2366

AN ANALOG STUDY OF A ROTATING-SOLID-ROCKET CONTROL SYSTEM AND ITS APPLICATION TO ATTITUDE CONTROL OF A SPACE-VEHICLE UPPER STAGE

By A. Thomas Young and Jack E. Harris
August 1964

Page 3, lines 17 to 24:

Change units of M_Y to ft-lb.

Change units of M_{Y_q} to $\frac{\text{ft-lb}}{\text{rad/sec}}$.

Delete M_{Y_r}.

Change units of M_Z to ft-lb.

Change units of M_{Z_r} to $\frac{\text{ft-lb}}{\text{rad/sec}}$.

Page 24: Change equations to read as follows (arrows indicate where changes are made):

$$m\dot{u} - mvr + mwq = F\left(\cos \delta_1 + \cos \delta_2 + \cos \delta_3 + \cos \delta_4\right) + T - mg \sin \theta + C_{X,0}\bar{q}A \tag{B1}$$

$$m\dot{v} - mwp + mur = -F\left(\sin \delta_1 + \sin \delta_3\right) + Ta + mg \sin \phi \cos \theta + C_{Y_\beta}\beta\bar{q}A \tag{B2}$$

$$m\dot{w} - muq + mvp = F\left(\sin \delta_2 + \sin \delta_4\right) + Tb + mg \cos \phi \cos \theta + C_{Z_\alpha}\alpha\bar{q}A \tag{B3}$$

$$\dot{q}I_Y + rpI_X - rpI_Z = -F\left(\sin \delta_2 + \sin \delta_4\right)\left(x_{cg} - x_q\right) + Td + M_{Y_q}q - C_{Z_\alpha}\alpha\bar{q}A\left(x_{cg} - x_{cp}\right) \tag{B5}$$

7 Oct 66
HMW

$$\dot{r}I_Z + pqI_Y - pqI_X = -F\left(\sin \delta_1 + \sin \delta_3\right)\left(x_{cg} - x_r\right) + Te + M_{Z_r}r$$
$$+ C_{Y_\beta}\beta\bar{q}A\left(x_{cg} - x_{cp}\right) \qquad \text{(B6)}$$

Page 33: In ordinate scales for $C_{X,0}$ and C_{Z_α}, C_{Y_β}, change values from positive to negative.

Page 35: In ordinate scale for M_{Y_q}, M_{Z_r}, change values from positive to negative.

NASA-Langley, 1966 Issued 9-12-66

AN ANALOG STUDY OF A ROTATING-SOLID-ROCKET CONTROL SYSTEM AND ITS APPLICATION TO ATTITUDE CONTROL OF A SPACE-VEHICLE UPPER STAGE

By A. Thomas Young and Jack E. Harris

Langley Research Center
Langley Station, Hampton, Va.

NATIONAL AERONAUTICS AND SPACE ADMINISTRATION

For sale by the Office of Technical Services, Department of Commerce,
Washington, D.C. 20230 -- Price $1.75

AN ANALOG STUDY OF A ROTATING-SOLID-ROCKET CONTROL SYSTEM AND ITS APPLICATION TO ATTITUDE CONTROL OF A SPACE-VEHICLE UPPER STAGE

By A. Thomas Young and Jack E. Harris
Langley Research Center

SUMMARY

A study of the characteristics of a control system employing rotating-solid-propellant rockets for control forces is presented. The particular control system studied was developed originally for the George C. Marshall Space Flight Center under a contract. An open-loop analysis as well as a closed-loop analysis of the control system is presented. The results of the open-loop analysis are given in the form of a nonlinear mathematical representation of the system's dynamic operation. This mathematical representation is used in the closed-loop study which is a guidance and control analysis of a typical vehicle system. The guidance and control analysis employs a guidance system simulation incorporating various nonlinearities present in the system, a three-dimensional trajectory simulation and six-degree-of-freedom rigid-body vehicle simulation, as well as the derived nonlinear simulation of the control system.

The nonlinear characteristics of the control system that significantly affect its performance as observed from the analysis are friction, actuator velocity limit, and a sine function of the control deflection angle. The results of the guidance and control analysis show that gains can be selected from a consideration of dynamic stability, steady-state accuracy, and reliability which would insure a satisfactory flight mission.

INTRODUCTION

Several types of control systems have been used for thrust vector and/or attitude control of rocket vehicle stages. Among these are jet vanes, jetavators, movable main rocket nozzles, secondary fluid injection, and auxiliary gas jets. Each of these systems causes a degradation of the vehicle performance due to their weight and has limited capabilities. Except for the auxiliary gas jet system, each must be developed as an integral part of the main rocket. Ever increasing size and complication of design of rocket vehicles makes it desirable to have a control system which can be developed independently of the main rocket. It would also be desirable to have the control system inherently capable of providing velocity control, retro thrust, and spin-up. Also, of course, minimum

performance degradation is desired. The study of a new concept in control systems, which possesses the previously mentioned attributes, is presented in this report. This system uses the thrust of auxiliary rotating-solid-propellant rockets for control forces. The particular system (ref. 1) analyzed in this report was developed under an NASA contract for the George C. Marshall Space Flight Center.

The purpose of this report is to present the results of an open-loop and a closed-loop study of this control system. The open-loop study consisted of experimentally determining the response of a dynamic model of the control system. The experimental data were analyzed and a simulation of the control system derived which had characteristics which closely duplicated the measured characteristics. The closed-loop study consisted of a guidance and control analysis of a typical rocket vehicle system made up of a space vehicle, a guidance system, and the control system of interest. Only the attitude control characteristics of the system were investigated in the closed-loop study.

The result of the open-loop study of the control system is given as a nonlinear differential equation of motion with the necessary numerical values needed to generate a solution. The results of the closed-loop analysis are presented as stability boundaries and phase plane plots. Time histories of pertinent vehicle, trajectory, and guidance and control system parameters for selected guidance gains and mission events are also presented. In addition, the effect of control system nonlinearities on vehicle system stability and accuracy is presented. Methods of improving the control system are also discussed.

The study was conducted with analog computation facilities.

SYMBOLS

A	reference area, sq ft
a,b	direction cosine used in computing thrust component along missile Y- and Z-axis, respectively, dimensionless
c,d,e	moment arm for thrust moment about missile X-, Y-, and Z-axis, respectively, ft
$C_{X,0}$	axial-force coefficient at zero flow incidence angle, dimensionless
C_Z	normal-force coefficient, dimensionless
C_{Z_α}	rate of change of normal-force coefficient with angle of attack, $\frac{\partial C_Z}{\partial \alpha}$, 1/radian
C_Y	side-force coefficient, dimensionless

C_{Y_β}	rate of change of side-force coefficient with angle of sideslip, $\frac{\partial C_Y}{\partial \beta}$, 1/radian
f	frequency, cps
F	nominal thrust of one control rocket multiplied by cos 10° (cant angle), lb
g	acceleration due to force of gravity, ft/sec^2
I_X, I_Y, I_Z	mass moment of inertia about X-, Y-, and Z-axis, respectively, slug-ft^2
K_2	control-subsystem internal-velocity feedback gain, volts/radian/sec
K_3	control-subsystem acceleration gain, radians/sec^2/volt
K_p, K_q, K_r	roll-, pitch-, and yaw-rate gain, volts/radian/sec
K_δ	control rocket position feedback gain, volts/radian
K_ϕ, K_θ, K_ψ	roll-, pitch-, and yaw-attitude gain, volts/radian
M	Mach number, dimensionless
m_f	frictional parameter, $\frac{\text{Frictional moment}}{\text{Inertia}}$, radians/sec^2
M_Y see errata	pitching moment, dimensionless
M_{Y_q} see errata	rate of change of pitching moment with pitching velocity, $\frac{\partial M_Y}{\partial q}$, ft-lb/radians/sec see errata
M_{Y_r} see errata	rate of change of pitching moment with yawing velocity, $\frac{\partial M_Y}{\partial r}$, ft-lb/radians/sec see errata
M_Z see errata	yawing moment, dimensionless
M_{Z_r} see errata	rate of change of yawing moment with yawing velocity, $\frac{\partial M_Z}{\partial r}$, ft-lb/radians/sec see errata
m	mass, slugs
p	rolling velocity, radians/sec
q	pitching velocity, radians/sec
$\bar{q}$	dynamic pressure, lb/sq ft

r	yawing velocity, radians/sec
S	Laplace variable, sec^{-1}
T	thrust of main rocket motor, lb
t	time, sec
u,v,w	component of missile linear velocity relative to earth along X-, Y-, and Z-axis, respectively, ft/sec
V	missile linear velocity relative to earth, ft/sec
V_s	velocity of sound, ft/sec
V_δ	voltage input to control system, volts
X,Y,Z	body axis of missile, dimensionless
x,y,z	distance along body axes, ft
X_E, Y_E, Z_E	earth-fixed axes, dimensionless
x_E, y_E, z_E	component of distance between missile center of gravity and earth-fixed axis along X_E-, Y_E-, and Z_E-axis, respectively, ft
X_R, Y_R, Z_R	reference axes, dimensionless
x_{cg}	center-of-gravity distance from nose, ft
x_{cp}	center-of-pressure distance from nose, ft
x_p	moment arm for control moment about X-axis, ft
x_q	distance of pitch-roll control rockets from nose, ft
x_r	distance of yaw-roll control rockets from nose, ft
α	angle of attack, radians
β	angle of sideslip, radians
δ	control-rocket deflection angle, radians
$\epsilon_\phi, \epsilon_\theta, \epsilon_\psi$	roll-, pitch-, and yaw-guidance-error signals, volts
η	flow incidence angle, radians

θ	pitch angle of missile relative to earth-fixed axes, deg
θ_R	reference pitch angle relative to earth-fixed axes, deg
θ_ϵ	pitch-attitude-error angle of missile relative to gyro reference axis, deg
ρ	free-stream static density, slug/ft^3
ϕ	roll angle of missile relative to earth-fixed axes, deg
ϕ_R	reference roll angle relative to earth-fixed axes, deg
ϕ_ϵ	roll-attitude-error angle of missile relative to gyro reference axes, deg
ψ	yaw angle of missile relative to earth-fixed axes, deg
ψ_R	reference yaw angle relative to earth-fixed axes, deg
ψ_ϵ	yaw-attitude-error angle of missile relative to gyro reference axes, deg
ω	frequency, radians/sec

Subscript:

0	initial value

Dots over symbols denote differentiation with respect to time. Primes indicate rate gyro output. The numbers 1, 2, 3, and 4 denote control rocket number 1, 2, 3, and 4, respectively, as shown in the following sketch:

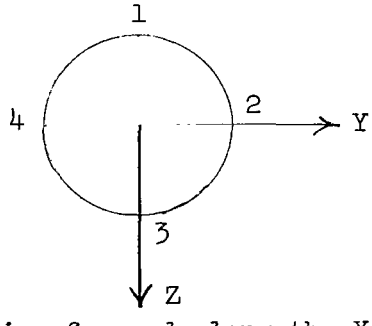

View looking forward along the X-axis

PHYSICAL DESCRIPTION AND CHARACTERISTICS

OF CONTROL SYSTEM AND VEHICLE

The closed-loop study of the rotating-solid-propellant-rocket control system was conducted on an analog computer utilizing simulations of systems of a typical two-stage rocket vehicle. For a flight application the thrust forces of the control system could be used to control the upper stage to predetermine roll, pitch, and yaw reference attitudes by using a position- and rate-sensing guidance system to provide the necessary reference and stability functions. This possible flight application represents the task studied. Each system of the typical vehicle is discussed in detail subsequently in this section.

Control System

The control system discussed in this report is an electrical-mechanical-chemical system which utilizes the thrust of four solid-propellant rockets for control power. The control system is pictorially shown in figure 1, and schematically shown mated with a space vehicle in figure 2. The control system is compactly designed to occupy a minimum volume which necessitates the unsymmetrical location of the control rockets as seen in figure 2. The solid-propellant control rockets are bearing mounted to allow rotation about axes parallel to the Y,Z plane shown in figure 2, and are equipped with canted nozzles that direct the thrust rearward and in planes nearly parallel to the longitudinal axis of the controlled vehicle. The control system is geometrically arranged such that rotation of two of the control rockets produces lateral components of thrust which provide pitch controlling moments. Rotation of the remaining two control rockets produces lateral components of thrust which provide yaw controlling moments. Roll control is obtained by differential deflection of the two pitch-control rockets and by differential deflection of the two yaw-control rockets. Thus, all four control rockets are employed for roll control.

The torque necessary to deflect each control rocket is produced by an electrical drive motor and is transmitted to the control rocket through mechanical gearing. A potentiometer, which provides control-rocket position feedback, is also geared to the control rocket. The control system consists of four identical and individual loops, each composed of a control rocket, electrical drive motor, feedback potentiometer, and gearing. The nominal thrust time history for one control rocket is given in figure 3. The electrical drive motor is voltage limited at 24 volts direct current. An additional feature of the control system is that the thrust of each control rocket can be partially or completely reduced at any point during its burn time. This reduction is accomplished by pyrotechnically opening a presized port directionally opposite the primary nozzle. The increased throat area results in a lower chamber pressure and thus an extension in the control rocket burn time and reduction in thrust. This feature could be advantageous in allowing a longer period of control. It should be noted that the control rocket thrust presented in figure 3 assumes continuous burning of the control rocket without reduction.

Research Vehicle

The research vehicle used in the analysis is a two-stage solid-propellant rocket vehicle and is shown in figure 4. The first-stage propulsion system consists of a Castor E-8 rocket motor and two Recruits. The second stage consists of an Antares rocket motor and a forward mounted spacecraft. The control rockets and their vulnerable accessories are protected during the critical ascending portion of flight by four ejectable fairings. The first stage of the research vehicle is used only as a booster to place the second stage into a suitable test environment.

The requirements of the test environment are such that disturbances shall not occur which exceed the capabilities of the control system. The trajectory parameters with $\pm 3\sigma$ deviations from launch to the approximate time of second-stage separation are given in figure 5. These parameters were used in selecting the exact separation time to satisfy the test-environment requirements.

Disturbances will result from dispersions and spin occurring during the unguided portion of flight, that is, prior to separation of the second stage. Thrust misalinement of the Antares may result in an additional disturbance. These disturbances are not intentional; however, they have a high probability of occurring. To insure that test disturbances are available, a programed attitude change is provided.

Second-Stage System

The second-stage system is the portion of the research vehicle which is of primary interest. As was previously indicated, only the second stage was considered to be guided by the control subsystem. It should be noted that previously in this report the control unit has been referred to as a system; in future discussion it is called a subsystem since it is considered to be a part of a vehicle system. A drawing of the second stage with pertinent dimensions is given in figure 2. The second-stage nominal aerodynamic, thrust, and mass characteristics which were used in the analysis are presented in figure 6. The aerodynamic quantities are based on a reference area of 1 square foot and the Antares thrust is for vacuum conditions.

The second-stage system consists of the combination of Antares and the spacecraft, and the control and guidance subsystems which are mounted in the spacecraft. A block diagram showing the integration of the individual subsystems into the complete second-stage system is presented in figure 7.

An existing guidance subsystem was chosen for use on the research vehicle. A purpose of the guidance and control analysis was to define the modifications required to adapt this guidance subsystem to the mission. The complete subsystem is described to provide a general familiarity, and the parts that directly bear on the analysis are discussed in greater detail.

The guidance subsystem shown in functional diagram form in figure 8 is composed of six basic units: the gyro package, the programer, the proportional

amplifier, the roll comparator, the demodulators, and the power supply. The basic function of the guidance subsystem is to sense the vehicle attitude and motion and to provide appropriate signals to the control subsystem to produce the desired stability and control characteristics. The guidance subsystem also provides properly sequenced and timed signals to initiate various in-flight events.

The gyro package consists of two 2-degree-of-freedom free gyros and three body-fixed rate gyros. The position gyro outputs are in the form of angle-off-null readings and gyro torque motors are provided to precess the gyros to the desired initial position relative to the launch attitude. Since the guidance subsystem is a null-seeking device, this procedure amounts to rotation of the null or reference axes.

The programer functions are providing timed or otherwise sequenced flight event signals, weighting and summing the respective rate signals from the gyro package with their corresponding attitude errors to produce combined error signals, and supplying these signals to the proportional amplifier. Gyro torque motor voltages for precessing the free gyros to the proper reference attitude axes are supplied by this unit. The flight event sequence and programed maneuver sequence are set in the programer when it is initially fabricated. Gyro torque motor voltage levels (to be applied prior to launch) may be inserted into the programer remotely from the launch checkout console by means of the umbilical connection.

The proportional amplifier accepts 400 cps error signals from the programer and provides proportional d-c voltage to the control subsystem drive motors. Control rocket position is taken from the control subsystem position feedback potentiometers and summed with the weighted errors from the programer at the appropriate point in the amplifier network.

The roll comparator samples roll-rate information from the gyro package and performs discriminating operations on this signal in order to initiate additional gyro precessing. This precessing is used to compensate for gyro drift caused by the unintentional and unpredictable rolling of the vehicle during first-stage burning.

DETERMINATION OF MATHEMATICAL MODEL OF CONTROL SUBSYSTEM

To simulate adequately the control subsystem discussed in this report, it was necessary to determine qualitatively and quantitatively the subsystem's characteristics both linear and nonlinear. The approach to obtaining this information was to determine analytically the performance of a linear mathematical model of the control subsystem and to compare this with experimental data generated from operation of a dynamic model of the control subsystem. The difference between the performances of the linear model and the dynamic model is an indication of the nonlinear characteristics. A mathematical representation of the control subsystem was obtained by modifying the linear description until the performance predicted by it matched that of the experimental data. An analog representation can be obtained from the mathematical description. The dynamic

model consists of duplicate electrical components, duplicate bearings, and simulated inertia of the research control subsystem and is therefore an operational duplicate. One loop of the dynamic model is pictorially presented in figure 9.

The linear representation of one of the four identical control subsystem loops is given by reference 1 as

$$\ddot{\delta} + K_2K_3\dot{\delta} = K_3V_\delta \tag{1}$$

where V_δ is the input voltage to the electrical drive motor and δ is the control-rocket deflection angle. The parameters K_2 and K_3 are functions of the dynamic characteristics of the electrical and mechanical components. Reference 1 presents the numerical values of K_2 and K_3 as $K_2 = 4.26 \frac{\text{volt}}{\text{radian/sec}}$; $K_3 = 5.17 \frac{\text{radians/sec}^2}{\text{volt}}$ at control rocket ignition; and $K_3 = 8.0 \frac{\text{radians/sec}^2}{\text{volt}}$ at control rocket burnout, with K_3 varying linearly with control rocket burn time because of the variation in inertia.

Equation (1) can be written in Laplace transform notation as

$$S^2(\delta) + K_2K_3S(\delta) = K_3V_\delta \tag{2}$$

from which the following transfer functions can be determined:

$$\frac{\delta}{V_\delta} = \frac{K_3}{S^2 + K_2K_3S} \tag{3}$$

$$\frac{\dot{\delta}}{V_\delta} = \frac{K_3}{S + K_2K_3} \tag{4}$$

The steady-state solutions of equations (3) and (4) for a sinusoidal driving function are given below in polar notation (see ref. 2):

$$\frac{\delta}{V_\delta} = \frac{1}{K_2\omega} \frac{1}{\sqrt{1 + \left(\frac{\omega}{K_2K_3}\right)^2}} \angle -90 + \tan^{-1}\frac{-\omega}{K_2K_3} \tag{5}$$

and

$$\frac{\dot{\delta}}{V_\delta} = \frac{1}{K_2} \frac{1}{\sqrt{1 + \left(\frac{\omega}{K_2K_3}\right)^2}} \angle \tan^{-1}\frac{-\omega}{K_2K_3} \tag{6}$$

The performance factors which were used in determining the control subsystem's nonlinear characteristics are the amplitude ratio and the control-rocket deflection rate, each as a function of input voltage and frequency. These parameters can be readily determined for the linear model from equations (5) and (6).

A plot of the variation of amplitude ratio with input voltage for three possible control subsystem operating frequencies is given in figure 10. The dotted lines are the results obtained from equation (5) for the linear model and the solid curves are from the experimental data obtained from the dynamic model. Considerable nonlinear effects are obvious from figure 10; however, the exact nature of the nonlinearities is not apparent. Figure 11 is a plot of the variation of steady-state control-rocket deflection rate with input voltage. Frequency variation has negligible effect on $\dot{\delta}$ within the frequency range of interest, namely, up to approximately 1 cycle per second. Inspection of equation (6) would indicate this fact. The dashed line in figure 11 represents the linear analytical data calculated from equation (6), and the solid lines represent the experimental data. Note that a 3.5-volt input is required before the nonlinear subsystem begins to respond and that it stalls at a 2.5-volt input when coming from a dynamic condition. When operating on the steady-state portion of the curve, no hysteresis was noted. The difference in starting and stopping input voltage and the near-constant control-rocket deflection-rate difference of about 30°/sec indicates nonlinear characteristics that might be expected for the type of system being investigated. The starting condition is obviously caused by starting or static friction and the steady-state velocity difference is apparently the effect of coulomb friction. Coulomb friction is a phenomenon usually present in mechanical systems and is independent of velocity variation.

An approximate representation of the assumed nonlinearities just discussed is presented in figure 12. The frictional parameter m_f, that is, $\frac{\text{Frictional moment}}{\text{Inertia}}$ is produced by the nonlinear frictional moment. The peak value of m_f, which is shown as b, for zero $\dot{\delta}$ corresponds to the subsystems starting friction and the lower plateau of $m_f = c$ represents the coulomb friction. The exact nature of the transient from starting to steady-state conditions is difficult to determine and for a realistic system probably very unrepeatable; therefore, only an engineering approximation was deemed to be practical for this study. The numerical values necessary to establish the magnitudes of a, b, and c and to define the transient from starting to steady-state conditions were obtained by a trial-and-error procedure. The equation of motion describing the linear model of the subsystem (eq. (1)) was modified to give the nonlinear equation

$$\ddot{\delta} + K_2K_3\dot{\delta} - m_f = K_3V_\delta \tag{7}$$

It is assumed in equation (7) that K_3 is constant. Equation (7) was programed on an analog computer and the numerical values and nature of the starting transient were varied until the variation of δ with V_δ duplicated that obtained

from the dynamic model for the frequency range of interest. In essence, it was necessary to match the nonlinear data given in figure 10. The numerical values of a, b, and c were determined to be as given in figure 12. It was determined that the characteristics of the transient from starting to steady-state conditions had no noticeable effect; therefore, the simplified representation shown in figure 12 was used. The solution of equation (7), utilizing the results given in figure 12, accurately represented the dynamic model's performance.

During the study of the control subsystem's nonlinear characteristics it was observed that the variation of K_3, which is a function of the inertia of the subsystem, had little or no effect on the performance predicted by the nonlinear analog model. It was therefore assumed to be constant at $K_3 = 7 \frac{\text{radians/sec}^2}{\text{volt}}$. Also apparent from the study was the validity of $K_2 = 4.26$ volt/radian/sec. The reciprocal of K_2 is the slope of the curve for the variation of $\dot{\delta}$ with V_δ and it can be seen in figure 11 that the slopes of the plots for the linear and nonlinear models are approximately the same within the steady-state region.

ANALOG SIMULATION

General

As previously stated, the purpose of the guidance and control analysis was to study analytically the problems associated with attitude control of a research-vehicle upper stage utilizing the research control subsystem. In order that predictable nonlinearities and dynamic coupling could be incorporated into the analysis, the study was conducted with the aid of an analog computer. The analog simulation was derived by considering the total second-stage system as being composed of the second-stage vehicle, the control subsystem, and the guidance subsystem as was symbolicly shown in figure 7. A diagram showing the manner in which the individual subsystems were mated in the analog simulation is given in figure 13, and a discussion of the simulation of each subsystem follows.

Control Subsystem Simulation

The analog simulation of the control subsystem used in the guidance and control analysis consisted of four identical and individual nonlinear servo loops. Each loop represented the dynamics involved in inducing control-rocket motion, and is mathematically described by the nonlinear equation of motion given as equation (7) in this report. The numerical values for K_2 and K_3 used in the solution of the equations were as previously given. The values for m_f are given in figure 12. The input voltage V_δ needed to excite the control subsystem simulation was supplied by the guidance simulation. The output from the control subsystem simulation δ was introduced into the simulation of the second-stage vehicle as well as into the guidance simulation. This relationship can be seen in figure 13.

Guidance Subsystem Simulation

The guidance subsystem simulation consists of a representation of the gyro outputs and a representation of the weighting and summing of the gyro outputs with the control position feedback parameters to define the inputs to the control subsystem.

The outputs of the attitude gyros are proportional to the sine of the gyro gimbal angles and are defined by equations derived in appendix A. The resulting equations which are in terms of Euler angles ϕ, θ, and ψ, determined by the second-stage vehicle and trajectory simulation, and an inertial pitch reference angle θ_R are as follows:

$$\sin \theta_\epsilon = \sin \theta \cos \theta_R - \cos \theta \cos \psi \sin \theta_R \tag{8}$$

$$\sin \psi_\epsilon = \cos \theta \sin \psi \tag{9}$$

$$\sin \phi_\epsilon = \frac{\sin \phi \sin \theta \cos \psi \sin \theta_R - \cos \phi \sin \psi \sin \theta_R + \sin \phi \cos \theta \cos \theta_R}{(1 - \sin^2 \theta_\epsilon)^{1/2}} \tag{10}$$

The outputs of the rate gyros are equivalent to the body rates p, q, and r while operating below the limiting or saturation value of the gyro. Body rates higher than the saturation value, which is 40° per second, will appear to the guidance subsystem as the saturation value. Thus, the simulation of the rate-gyro outputs consist of monitoring and limiting when necessary the body rates determined by the vehicle and trajectory simulation.

The control subsystem forcing functions are defined by the following expressions:

$$V_{\delta_1} = \epsilon_\psi + \epsilon_\phi - K_\delta \delta_1 \tag{11}$$

$$V_{\delta_2} = \epsilon_\theta - \epsilon_\phi - K_\delta \delta_2 \tag{12}$$

$$V_{\delta_3} = \epsilon_\psi - \epsilon_\phi - K_\delta \delta_3 \tag{13}$$

$$V_{\delta_4} = \epsilon_\theta + \epsilon_\phi - K_\delta \delta_4 \tag{14}$$

where

$$\epsilon_\theta = K_\theta \sin \theta_\epsilon + K_q q' \tag{15}$$

$$\epsilon_\psi = K_\psi \sin \psi_\epsilon + K_r r' \tag{16}$$

$$\epsilon_\phi = K_\phi \sin \phi_\epsilon + K_p p' \tag{17}$$

The guidance subsystem simulation is schematically shown as a portion of figure 13.

Second-Stage Vehicle and Trajectory Simulation

The second-stage vehicle and trajectory simulation used in the guidance and control analysis was rigorous in that the trajectory simulation was three dimensional and the vehicle representation was in six degrees of freedom. The simulation is a simplified version of the simulation presented in reference 3 and is given in appendix B. It was assumed that the research vehicle was mass balanced such that the products of inertia could be neglected.

The sine of the control-rocket deflection angle noted in the vehicle equations of motion (see appendix B) is an additional nonlinear characteristic peculiar to the control concept under investigation.

The representation of the vehicle's equations of motion is dependent upon the control subsystem simulation for the magnitudes and directions of the four control rocket deflection angles. The angular attitudes and rates of the vehicle determined by the vehicle and trajectory simulation are inputs to the guidance subsystem simulation. (See fig. 13.)

ANALYSIS AND RESULTS

Method of Analysis

The guidance and control analysis was conducted to determine magnitudes for the various system variables such that a satisfactory flight mission could be conducted. The variables that are available to shape the flight characteristics are time or altitude of second-stage separation, control-rocket deflection limit and the weighting factors associated with the outputs of the rate and attitude gyros and the control-position feedback loops. It is obvious that a variation of each variable will in turn affect the selection of remaining variables; therefore, an iteration process was necessary to determine a satisfactory value for each parameter. The study was conducted with the aid of an analog computer utilizing the nonlinear simulations previously discussed.

The analysis was conducted by assuming the flight to be divided into two separate phases, each associated with a specific method of control. This approach was used since until the vehicle is alined to the proper roll reference, the pitch- and yaw-attitude error information from the free gyros is not suitable for direct use in the body-axis-oriented control subsystem without compensation for the transformation between the instantaneous measurement axis and the control application axis. Thus, initially only rate control can be established about the pitch and yaw axes. The initial phase or initial roll capture maneuver consists of removing any induced roll rate and orienting the vehicle to the proper roll reference attitude. For this maneuver, pitch- and yaw-rate control as well as roll-rate and attitude control are used.

Upon achieving the desired roll reference attitude, pitch- and yaw-attitude information must be added to achieve the desired three-axes stabilization. The second-phase or three-axis attitude control maneuver consists of orientating the vehicle to the selected pitch and yaw reference attitudes and maintaining this reference until 25 seconds after Antares ignition, at which time the pitch gyros were precessed to give a 5° reference change. The purpose of this reference change was to provide a known disturbance. This new reference was maintained throughout the remaining portion of the controlled flight. Each maneuver is discussed in more detail subsequently.

Since the process used in determining the variables is repetitious and results in a large accumulation of data, it is practical to present only a portion of the process in this report. The data presented are concerned with the final selection of attitude and rate gains and is based on a pre-selected separation time of 80 seconds, control-rocket deflection limit of 60°, and control position feedback gain of 100 volts/radian.

Initial Conditions

The selected separation altitude at 80 seconds is 220,000 feet and corresponds to the 3σ low trajectory. This trajectory was considered to be critical and was used in the analysis since it gives the highest resulting dynamic pressure and thus the highest unstable aerodynamic moment. The initial magnitudes of the horizontal and lateral ranges did not affect the problem and were assumed to be zero. The initial velocity is 3,400 feet per second from figure 5.

A plot of the 3σ booster roll rate is given in figure 14. The selected separation time fixed the maximum expected roll rate at ± 2.43 radians/sec. The pitch and yaw angular rates at 80 seconds were small and were neglected.

The second-stage attitude references are based on a nominal trajectory; therefore, the roll and yaw references can be taken as zero. Figure 14 gives the variation of the pitch angle with time from launch. The established separation time results in a nominal pitch-attitude reference of 60.5°. The initial pitch and yaw attitudes were established to be 36.5° and 25.1°, respectively, by using equations (8) and (9) with a 20° yaw error and a 20° pitch error. These pitch- and yaw-attitude errors were determined from an analysis of errors produced by dispersions and angle-of-attack amplification due to roll-pitch resonance during first-stage coast as well as to an effective error due to gyro drift. The initial roll attitude is not predictable and was varied, as will be subsequently discussed.

The 1962 U.S. Standard Atmosphere (ref. 4) was used in the analysis.

Initial Roll Capture Maneuver

The gains which are available to shape the roll capture maneuver are the gain on the roll rate K_p and the gain on the roll attitude K_ϕ if the pitch and yaw rate gains are considered to be fixed. The criteria for selecting a

satisfactory set of gains was time to complete the maneuver and completion of the maneuver with minimum overshoot and minimum control reversals.

The control error law applicable to roll control is given by equation (17) and is as follows:

$$\epsilon_{\phi} = K_{\phi} \sin \phi_{\epsilon} + K_p p'$$

and p' is related to p by the following relationships:

$$p < C \qquad p' = p$$

$$p > C \qquad p' = C$$

where C represents the saturation value of the rate gyro. For the rate gyro of the guidance subsystem, the saturation value is 0.7 radian per second; thus, the solution to equation (17) is discontinuous for vehicle roll rates higher than this value. Equation (17) indicates that a ratio of rate gain to attitude gain greater than 1.43 is needed to generate a zero-error solution that stays within the linear region of the rate gyro.

Vehicle response motions were determined for various combinations of attitude and rate gain values in an effort to obtain a satisfactory maneuver. Figure 15 shows the phase plane trajectories of the motion involved in completing the initial maneuver from an initial roll rate of 2.43 radians per second and various initial roll attitudes incorporating several combinations of rate and attitude gain values. The maneuver consists of reducing the roll rate to zero and orientating the vehicle to a zero roll attitude reference. The vehicle attitude error was eliminated by rolling the vehicle clockwise or counterclockwise depending upon the quadrant in which the roll rate became zero. It was for this reason that some trajectories ended at $\phi = 0^{\circ}$ and others at $\phi = 360^{\circ}$. The dashed curves shown in figure 15 represent solutions of equation (17). The discontinuities in the curves are due to the saturation level of the rate gyro. Parts (a), (b), and (c) of figure 15 can be used to compare the effect of changing the ratio of rate to attitude gain through the region 1 to 1.5 while maintaining the attitude gain equal to 200 volts/radian. Parts (d), (e), and (f) of figure 15 are for the same gain ratios but the attitude gain is 600 volts/radian. From comparing parts (a) and (d) of figure 15, it is evident that the trajectory excursions from the zero-error curve are considerably greater for the higher value of attitude gain. Although the excursions are quite comparable for parts (c) and (f) of figure 15, more control reversals are associated with the higher attitude gain. This is more clearly shown in figure 16 which shows time histories of the control-rocket angular positions and angular rates. Figure 15 indicates that a ratio of rate gain to attitude gain greater than 1 with an attitude gain less than 600 volts per radian appears desirable for the initial maneuver.

Three-Axis Attitude Control

The major criteria of system operation during three-axis control are static accuracy and dynamic stability. The roll, pitch, and yaw attitude and rate gains are available to establish satisfactory dynamic performance. The second-stage system exhibits type 0 servo-system steady-state characteristics (ref. 5); that is, in order to produce a steady control deflection to balance a steady external moment, a steady actuating (attitude) error must be present. Therefore, the three-axis attitude gains dictate the degree of static accuracy. Since the attitude gains are used to shape two parameters, a "trade-off" is apparent.

The static accuracy or steady static error $\theta_{e,ss}$ resulting from a thrust misalinement moment M_t can be determined from the following expression:

$$\theta_{e,ss} = \frac{M_t}{\frac{2F(x_{cg} - x_q)}{K_\theta / K_\delta}} \tag{18}$$

Equation (18) is written for the pitch plane; however, with substitution of the proper variables the same equation applies to the roll and yaw planes if all four control rockets are used for roll control. Figure 17 shows the steady-state attitude error required to produce a control moment sufficient to balance a 250 foot-pound pitch thrust misalinement moment and a 25 foot-pound roll thrust misalinement moment as a function of pitch- and roll-attitude gains. To obtain the maximum error, a pitch-control moment of 515 foot-pounds and a roll-control moment of 274 foot-pounds, which occur at Antares burnout, were used in the calculations. It can be seen from figure 17 that the steady-state attitude error increases as the attitude gain decreases.

Figures 18 and 19 show the dynamic stability boundaries as functions of attitude and rate gain for the roll and pitch planes. The yaw-plane stability boundary encompassed slightly more area than the pitch plane because of a shorter control moment arm and is not shown. In addition to showing the boundaries as functions of system gains, the effects of variations of certain vehicle and control subsystem parameters on the boundaries are shown.

Figure 18 shows the stability boundary associated with the roll plane. The pitch and yaw attitude and rate gains were held constant while the roll gains were varied. The point in flight where instability was encountered varied considerably. The left-hand boundary was associated with initial vehicle instability. The system was so lightly damped that it could not perform the initial orientation and the vehicle diverged while attempting to orient itself. The right-hand boundary was encountered at or near second-stage burnout. The decrease in inertia along with the burnout transient was sufficient to at least make the system unusable since the control rocket subsystem would break into a limit cycle of sufficient amplitude to make it worthless for control use.

The dashed right-hand curve indicates the amount of reduction associated with a 10-percent decrease in the roll inertia of the vehicle or a 10-percent increase in the control rocket thrust. The region between the left-hand

boundaries represents stable operation; however, the response of the vehicle to commands is so lightly damped as to be unusable from practical considerations. The decrease in roll inertia had no measureable effect on the left-hand boundary.

Figure 19 shows the stability boundary associated with the pitch plane. This curve was obtained in a manner similar to that used for the roll-plane analysis. Again, the left-hand boundary was associated with divergence encountered in the attempt at initial orientation, and the right-hand boundary was associated with instability induced by control rocket subsystem limit cycle operation. The effect of a 10-percent decrease in pitch inertia or a 10-percent increase in the control rocket thrust is indicated by the dashed line. The effect of a 25-percent reduction in control-rocket deflection rate on the usable gain region is also shown.

In addition to studying the effects of a 25-percent reduction in deflection rate, the effect on vehicle performance of unsymmetric deflection rates was also studied. The deflection rate for one control rocket in each of the pitch and yaw pairs was increased 20 percent over the nominal rate and the other was reduced to 20 percent below nominal. This condition induced a minor amount of roll motion while correcting pitch or yaw errors; however, the motion was insignificant and quickly eliminated when attitude and rate gains with significant gain margins were used.

Gain Selection

The attitude and rate gains for the second-stage system were selected to give desirable stability characteristics with reasonable accuracy and high reliability. The steady-state accuracy was somewhat compromised for reliability. It was considered that the reliability could be increased by having a minimum number of gain changes and selecting gains which would prevent excessive limiting oscillations of the control rockets. The gains selected are as follows:

K_{ϕ} = 200 volts/radian (t = 80 to t = 95 seconds)

K_{ϕ} = 600 volts/radian (t = 95 + seconds)

K_{θ} = 2000 volts/radian

K_{ψ} = 2000 volts/radian

K_{p} = 250 volts/radian/sec

K_{q} = 1300 volts/radian/sec

K_{r} = 1300 volts/radian/sec

Time histories of the pertinent vehicle, trajectory, guidance subsystem, and control subsystem parameters for the aforementioned gains and selected

mission events are given in figure 20. The initial roll capture maneuver begins at a time of 80 seconds and 15 seconds is allowed for completion of the maneuver. It is noted that the roll angle ϕ is not reduced to zero; however, the roll error angle ϕ_ϵ is zero. This condition is caused by geometric coupling due to the presence of pitch and yaw errors and can be seen by inspection of equation (10). Beginning at 95 seconds, 5 seconds is allowed for full 3-axes control which is followed by Antares ignition at 100 seconds. Toward the end of Antares burning (t = 125 seconds), a programed 5° pitch-attitude change occurs. The Antares burnout occurs at 141.6 seconds and the burnout of the control rockets occurs at 168 seconds. These time histories represent a predicted complete flight mission.

DISCUSSION

The control concept studied in this report has been shown to exhibit the following nonlinear characteristics:

(1) Friction
  (a) Starting
  (b) Coulomb

(2) Drive motor voltage limit

(3) Sine variation of control force

The sine variation of the control force is a fixed characteristic of the control concept investigated; however, the actuator limitation and friction can be varied in magnitude by design. The drive-motor voltage limitation is critical to the performance of control subsystem only in its effect upon the control deflection rate, which in turn affects the stability boundaries.

Effect of Nonlinearities on Stability and Accuracy

Figure 21 is a combination plot of the pitch stability boundary and the steady-state accuracy variation with attitude gain. The large region of stability is for a completely linear system and was calculated by using Routh's stability criteria. (See ref. 6.) The smaller boundary is the nominal data for the nonlinear system as was given in figure 19. The accuracy curve is the same as was presented in figure 17. It is obvious that the nonlinearities considered in this report have a significant effect upon the stability boundary area and this in turn upon the accuracy to which the research-vehicle second stage can be flown. As an example of the effect upon accuracy, the maximum value of K_θ for stable operation of the nonlinear system is 9100 volts/radian which corresponds to a steady-state error of 0.31°. For stable operation of the linear system, the maximum value of K_θ is 24,300 volts/radian which gives a steady-state error of 0.11°. This difference is even more pronounced for a selection of K_θ within the stability regions.

Figures 22 and 23 give an indication of the effect of the control-deflection-rate limit and the frictional nonlinearities separately. Figure 22 shows the pitch stability boundaries as were given in figure 21 along with an additional boundary representing a 100-percent increase in the control deflection rate. This condition is comparable to a 100-percent increase in the slope of the curve presented in figure 11. The rate increase is synonymous with employing a higher response actuator and the results are apparent from the figure. A comparison between the pitch stability boundary with and without friction is given in figure 23.

From a review of the results given in figures 21, 22, and 23, it can be concluded that for the guidance and control subsystem concept defined in this report, actuator selection and mechanical design could increase the stability boundary area and thus the steady-state accuracy. Even with the elimination of friction and a 100-percent increase in $\dot{\delta}$, there remains a large difference between this modified nonlinear stability boundary and the linear boundary.

The effect of activation of the previously discussed thrust-reduction feature upon the system stability was not studied since it can be qualitatively determined by investigation of figures 18 and 19. From these figures it can be seen that an increase in the control rocket thrust reduces the stability boundary and conversely a decrease in thrust can be expected to increase the region of stability. Since the thrust is reduced, the stability requirement is less stringent for the thrust-reduction maneuver than for the other portions of flight.

System Improvements

Two methods of improving the system performance in the area of static accuracy by changing the previously described subsystems readily come to mind. One means involves the addition of a signal proportional to the integral of the forward loop error signal in the error loop and thereby a change of the system operation to a type 1 servo system. (See ref. 5.) The integration of the error signal provides the signal that will produce the required control deflection to null any disturbance and thus eliminates the steady-state attitude error. The addition is not practical from hardware considerations with the present guidance subsystem and was not studied.

The second method involves increasing the stability region of the control subsystem through the use of control rocket deflection rate as an additional feedback quantity in the control servo loop. By increasing the stability region, higher values of attitude gain could be used and thereby reduce the steady-state-error—control-rocket-deflection relationship. Figure 24 compares the roll stability boundaries associated with two different amounts of control-rocket deflection rate feedback gain with those of the basic system. The final maneuver described earlier represented the reference for the study. The area of greatest improvement appears to be in the increased allowable rate gain rather than in the attitude gain. However, this increase in rate gain does enable the guidance subsystem to operate at a similar ratio of rate gain to attitude gain but for a larger attitude gain. This effect is shown by the dashed line representing a ratio of rate to attitude gain of 0.5. The maximum attitude gain for the basic

system is 810 volts/radian while the maximum gain value is increased to 1,370 volts/radian for an addition of 10 volts/radian/second feedback signal in the servo loop. Therefore, the addition of control-rocket deflection rate feedback would improve the control concept studied in this report.

CONCLUDING REMARKS

The methodology used in studying the control subsystem discussed in this report points out the subsystem's nonlinear characteristics and the manner in which these nonlinear effects can be incorporated into a mathematical simulation. The nonlinear representation is used in a guidance and control analysis of a typical rocket vehicle. The results of the guidance and control analysis shows that there is a "trade-off" between stability and accuracy for the system considered. It was shown, however, that values for the variable parameters are available which will insure a satisfactory flight mission.

The effect of the observed control subsystem nonlinearities upon the vehicle system stability and accuracy was shown. Methods of improving the system were also discussed.

Langley Research Center,
National Aeronautics and Space Administration,
Langley Station, Hampton, Va., February 27, 1964.

APPENDIX A

DETERMINATION OF GYRO ANGLES IN TERMS OF EULER ANGLES AND A PITCH REFERENCE ANGLE

The gyro angles θ_ϵ, ψ_ϵ, and ϕ_ϵ were derived in terms of Euler angles θ, ψ, and ϕ and a pitch reference angle θ_R by using a series of orthogonal matrix transformations. The initial transformation is between the earth-fixed axes X_E, Y_E, and Z_E and the body axes of the missile X, Y, and Z. This transformation is as follows:

$$\begin{bmatrix} X \\ Y \\ Z \end{bmatrix} = \begin{bmatrix} 1 & 0 & 0 \\ 0 & \cos\phi & \sin\phi \\ 0 & -\sin\phi & \cos\phi \end{bmatrix} \begin{bmatrix} \cos\theta & 0 & -\sin\theta \\ 0 & 1 & 0 \\ \sin\theta & 0 & \cos\theta \end{bmatrix} \begin{bmatrix} \cos\psi & \sin\psi & 0 \\ -\sin\psi & \cos\psi & 0 \\ 0 & 0 & 1 \end{bmatrix} \begin{bmatrix} X_E \\ Y_E \\ Z_E \end{bmatrix} \tag{A1}$$

which, when simplified, becomes

$$\begin{bmatrix} X \\ Y \\ Z \end{bmatrix} = \begin{bmatrix} \cos\theta\cos\psi & \cos\theta\sin\psi & -\sin\theta \\ \sin\phi\sin\theta\cos\psi - \cos\phi\sin\psi & \sin\phi\sin\theta\sin\psi + \cos\phi\cos\psi & \sin\phi\cos\theta \\ \cos\phi\sin\theta\cos\psi + \sin\phi\sin\psi & \cos\phi\sin\theta\sin\psi - \sin\phi\cos\psi & \cos\phi\cos\theta \end{bmatrix} \begin{bmatrix} X_E \\ Y_E \\ Z_E \end{bmatrix} \tag{A2}$$

A transformation between the earth-fixed axes and the reference axes X_R, Y_R, and Z_R is given as equation (A3). This transformation is valid for a constant pitch reference, zero yaw reference, and zero roll reference.

$$\begin{bmatrix} X_R \\ Y_R \\ Z_R \end{bmatrix} = \begin{bmatrix} \cos\theta_R & 0 & -\sin\theta_R \\ 0 & 1 & 0 \\ \sin\theta_R & 0 & \cos\theta_R \end{bmatrix} \begin{bmatrix} X_E \\ Y_E \\ Z_E \end{bmatrix} \tag{A3}$$

By transposing, the following relation can be obtained:

$$\begin{bmatrix} X_E \\ Y_E \\ Z_E \end{bmatrix} = \begin{bmatrix} \cos\theta_R & 0 & \sin\theta_R \\ 0 & 1 & 0 \\ -\sin\theta_R & 0 & \cos\theta_R \end{bmatrix} \begin{bmatrix} X_R \\ Y_R \\ Z_R \end{bmatrix} \tag{A4}$$

Equation (A4) can be substituted into equation (A2) to give the following equation, which is the transformation between the body axis and the reference axes in terms of θ, ψ, ϕ, and θ_R.

$$\begin{bmatrix} X \\ Y \\ Z \end{bmatrix} = \begin{bmatrix} \cos\theta\cos\psi\cos\theta_R + \sin\theta\sin\theta_R & \cos\theta\sin\psi & \cos\theta\cos\psi\sin\theta_R - \sin\theta\cos\theta_R \\ \sin\phi\sin\theta\cos\psi\cos\theta_R - \cos\phi\sin\psi\cos\theta_R - \sin\phi\cos\theta\sin\theta_R & \sin\phi\sin\theta\sin\psi + \cos\phi\cos\psi & \sin\phi\sin\theta\cos\psi\sin\theta_R - \cos\phi\sin\psi\sin\theta_R + \sin\phi\cos\theta\cos\theta_R \\ \cos\phi\sin\theta\cos\psi\cos\theta_R + \sin\phi\sin\psi\cos\theta_R - \cos\phi\cos\theta\sin\theta_R & \cos\phi\sin\theta\sin\psi - \sin\phi\cos\psi & \cos\phi\sin\theta\cos\psi\sin\theta_R + \sin\phi\sin\psi\sin\theta_R + \cos\phi\cos\theta\cos\theta_R \end{bmatrix} \begin{bmatrix} X_R \\ Y_R \\ Z_R \end{bmatrix} \tag{A5}$$

The transformation between the body axes and the reference axes can be written in terms of gyro angles as follows:

$$\begin{bmatrix} X \\ Y \\ Z \end{bmatrix} = \begin{bmatrix} \cos\theta_\epsilon\cos\psi_\epsilon^* & \cos\theta_\epsilon\sin\psi_\epsilon^* & -\sin\theta_\epsilon \\ \sin\phi_\epsilon\sin\theta_\epsilon\cos\psi_\epsilon^* - \cos\phi_\epsilon\sin\psi_\epsilon^* & \sin\phi_\epsilon\sin\theta_\epsilon\sin\psi_\epsilon^* + \cos\phi_\epsilon\cos\psi_\epsilon^* & \sin\phi_\epsilon\cos\theta_\epsilon \\ \cos\phi_\epsilon\sin\theta_\epsilon\cos\psi_\epsilon^* + \sin\phi_\epsilon\sin\psi_\epsilon^* & \cos\phi_\epsilon\sin\theta_\epsilon\sin\psi_\epsilon^* - \sin\phi_\epsilon\cos\psi_\epsilon^* & \cos\phi_\epsilon\cos\theta_\epsilon \end{bmatrix} \begin{bmatrix} X_R \\ Y_R \\ Z_R \end{bmatrix} \tag{A6}$$

Since the gyro angle is measured in the plane of the missile and the yaw angle ψ^* noted in the transformation is the projection of the gyro yaw angle in the reference X_R, Y_R plane, the following expression is necessary to define the gyro yaw angle:

$$\sin \psi_\epsilon = \sin \psi_\epsilon{}^* \cos \theta_\epsilon \tag{A7}$$

From the transformations given in equations (A5) and (A6), the following simultaneous equations can be written by inspection:

$$-\sin \theta_\epsilon = \cos \theta \cos \psi \sin \theta_R - \sin \theta \cos \theta_R \tag{A8}$$

$$\sin \phi_\epsilon \cos \theta_\epsilon = \sin \phi \sin \theta \cos \psi \sin \theta_R - \cos \phi \sin \psi \sin \theta_R + \sin \phi \cos \theta \cos \theta_R \tag{A9}$$

$$\sin \psi_\epsilon{}^* \cos \theta_\epsilon = \cos \theta \sin \psi \tag{A10}$$

These equations can be rearranged and combined with equation (A7) to give the following gyro expressions:

$$\sin \theta_\epsilon = \sin \theta \cos \theta_R - \cos \theta \cos \psi \sin \theta_R \tag{A11}$$

$$\sin \psi_\epsilon = \cos \theta \sin \psi \tag{A12}$$

$$\sin \phi_\epsilon = \frac{\sin \phi \sin \theta \cos \psi \sin \theta_R - \cos \phi \sin \psi \sin \theta_R + \sin \phi \cos \theta \cos \theta_R}{\left(1 - \sin^2 \theta_\epsilon\right)^{1/2}} \tag{A13}$$

APPENDIX B

EQUATIONS DESCRIBING VEHICLE AND TRAJECTORY SIMULATION

The following equations describe the vehicle and trajectory simulation:

$$m\dot{u} - mvr + mwq = F\left(\cos \delta_1 + \cos \delta_2 + \cos \delta_3 + \cos \delta_4\right) + T - mg \sin \theta + C_{X,0}\bar{q}A \tag{B1}$$

$$m\dot{v} - mwp + mur = -F\left(\sin \delta_1 + \sin \delta_3\right) + Ta + mg \sin \phi \cos \theta + C_{Y_\beta}\beta\bar{q}A \tag{B2}$$

$$m\dot{w} - muq + mvp = F\left(\sin \delta_2 + \sin \delta_4\right) + Tb + mg \cos \phi \cos \theta + C_{Z_\alpha}\alpha\bar{q}A \tag{B3}$$

$$\dot{p}I_X = -F\left(\sin \delta_1 - \sin \delta_3 - \sin \delta_2 + \sin \delta_4\right)x_p + Tc \tag{B4}$$

$$\dot{q}I_Y + rpI_X - rpI_Z = -F\left(\sin \delta_2 + \sin \delta_4\right)\left(x_{cg} - x_q\right) + Td + M_{Y_q}q - C_{Z_\alpha}\alpha\bar{q}A\left(x_{cg} - x_{cp}\right) \tag{B5}$$

$$\dot{r}I_Z + pqI_Y - pqI_X = -F\left(\sin \delta_1 + \sin \delta_3\right)\left(x_{cg} - x_r\right) + Te + M_{Z_r}r + C_{Y_\beta}\beta\bar{q}A\left(x_{cg} - x_{cp}\right) \tag{B6}$$

$$\alpha = \frac{w}{u} \tag{B7}$$

$$\beta = \frac{v}{u} \tag{B8}$$

$$\eta = \frac{\sqrt{v^2 + w^2}}{u} \tag{B9}$$

$$\bar{q} = \frac{1}{2}\rho V^2 \tag{B10}$$

$$V = \sqrt{u^2 + v^2 + w^2} \tag{B11}$$

$$M = \frac{V}{V_s} \tag{B12}$$

$$\dot{\psi} = \frac{q \sin \phi + r \cos \phi}{\cos \theta} \tag{B13}$$

$$\dot{\phi} = p + \dot{\psi} \sin \theta \tag{B14}$$

$$\dot{\theta} = q \cos \phi - r \sin \phi \tag{B15}$$

$$\psi = \int_t \dot{\psi} \, dt + \psi_0 \tag{B16}$$

$$\phi = \int_t \dot{\phi} \, dt + \phi_0 \tag{B17}$$

$$\theta = \int_t \dot{\theta} \, dt + \theta_0 \tag{B18}$$

$$\dot{x}_E = u(\cos \theta \cos \psi) + v(\cos \psi \sin \phi \sin \theta - \sin \psi \cos \phi) + w(\cos \psi \cos \phi \sin \theta + \sin \psi \sin \phi) \tag{B19}$$

$$\dot{y}_E = u(\cos \theta \sin \psi) + v(\sin \psi \sin \phi \sin \theta + \cos \psi \cos \phi) + w(\sin \psi \cos \phi \sin \theta - \cos \psi \sin \phi) \tag{B20}$$

$$\dot{z}_E = -u(\sin \theta) + v(\sin \phi \cos \theta) + w(\cos \theta \cos \phi) \tag{B21}$$

$$x_E = \int_t \dot{x}_E \, dt + x_{E,0} \tag{B22}$$

$$y_E = \int_t \dot{y}_E \, dt + y_{E,0} \tag{B23}$$

$$z_E = \int_t \dot{z}_E \, dt + z_{E,0} \tag{B24}$$

REFERENCES

1. Fall, R. C., Koch, R. L., and DeBord, C. J.: Development of the Rocket Velocity and Attitude Control System - Final Summary Report. Eng. Dept. Rep. No. 2137 (Contract No. NAS 5-483), Allison Div., General Motors Corp., May 29, 1961.

2. Chestnut, Harold, and Mayer, Robert W.: Servomechanisms and Regulating System Design. Vol. I. John Wiley & Sons, Inc., c.1951.

3. James, Robert L., Jr. (With Appendix by Norman L. Crabill): A Three-Dimensional Trajectory Simulation Using Six Degrees of Freedom With Arbitrary Wind. NASA TN D-641, 1961.

4. Anon.: U.S. Standard Atmosphere, 1962. NASA, U.S. Air Force, and U.S. Weather Bureau, Dec. 1962.

5. Nixon, Floyd E.: Principles of Automatic Controls. Prentice-Hall, Inc., c.1953.

6. Perkins, Courtland D., and Hage, Robert E.: Airplane Performance Stability and Control. John Wiley & Sons, Inc., c.1949.

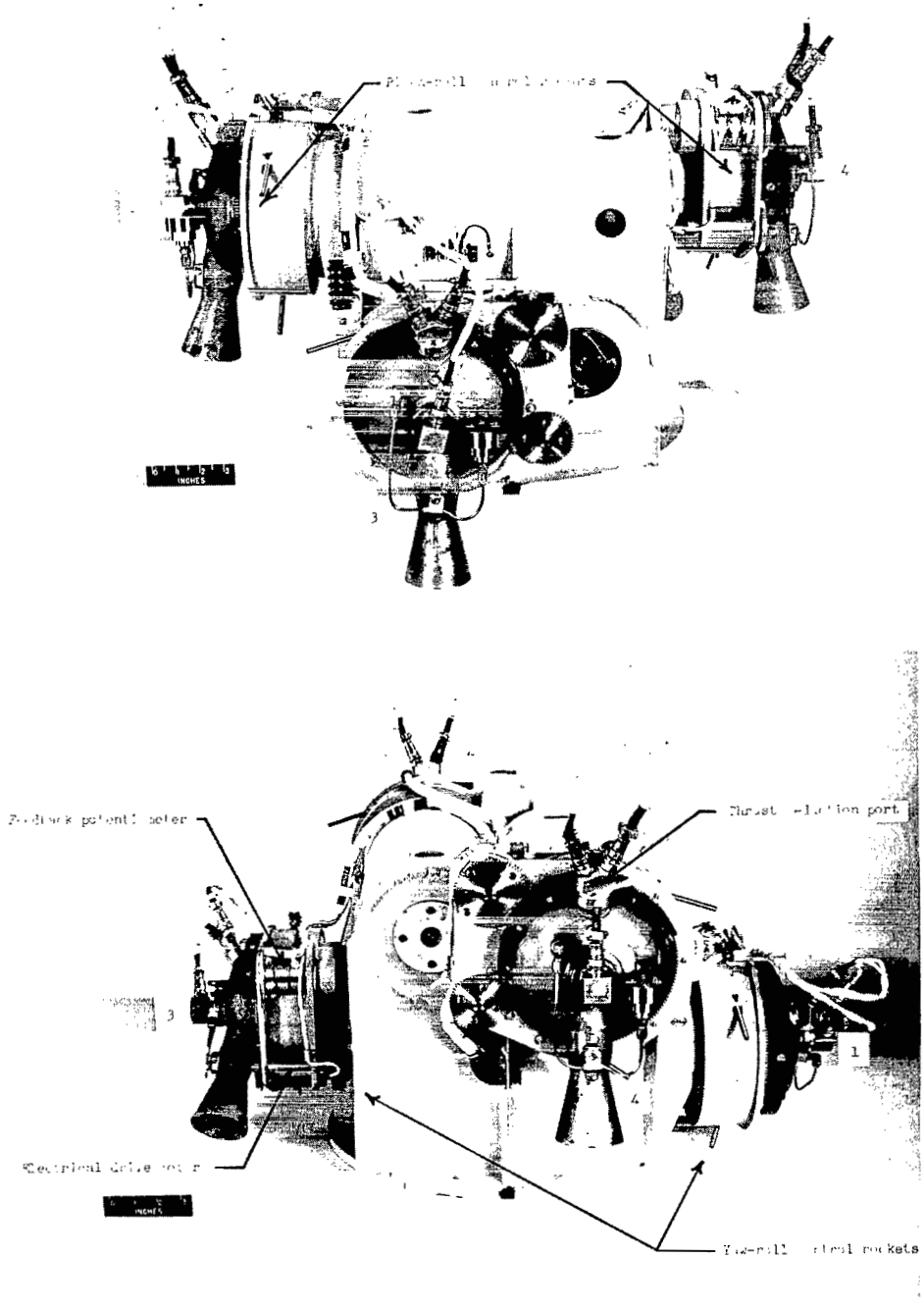

L-64-419

Figure 1.- Control system. Numbers designate control rockets.

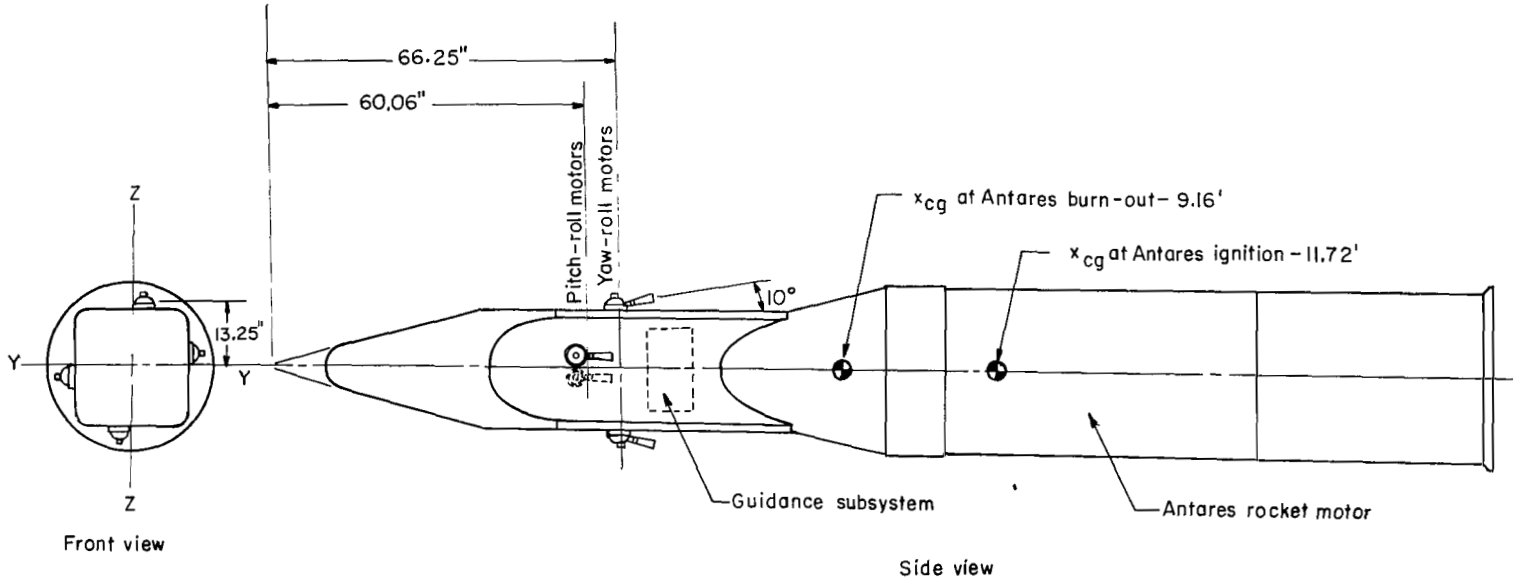

Figure 2.- Research-vehicle second stage.

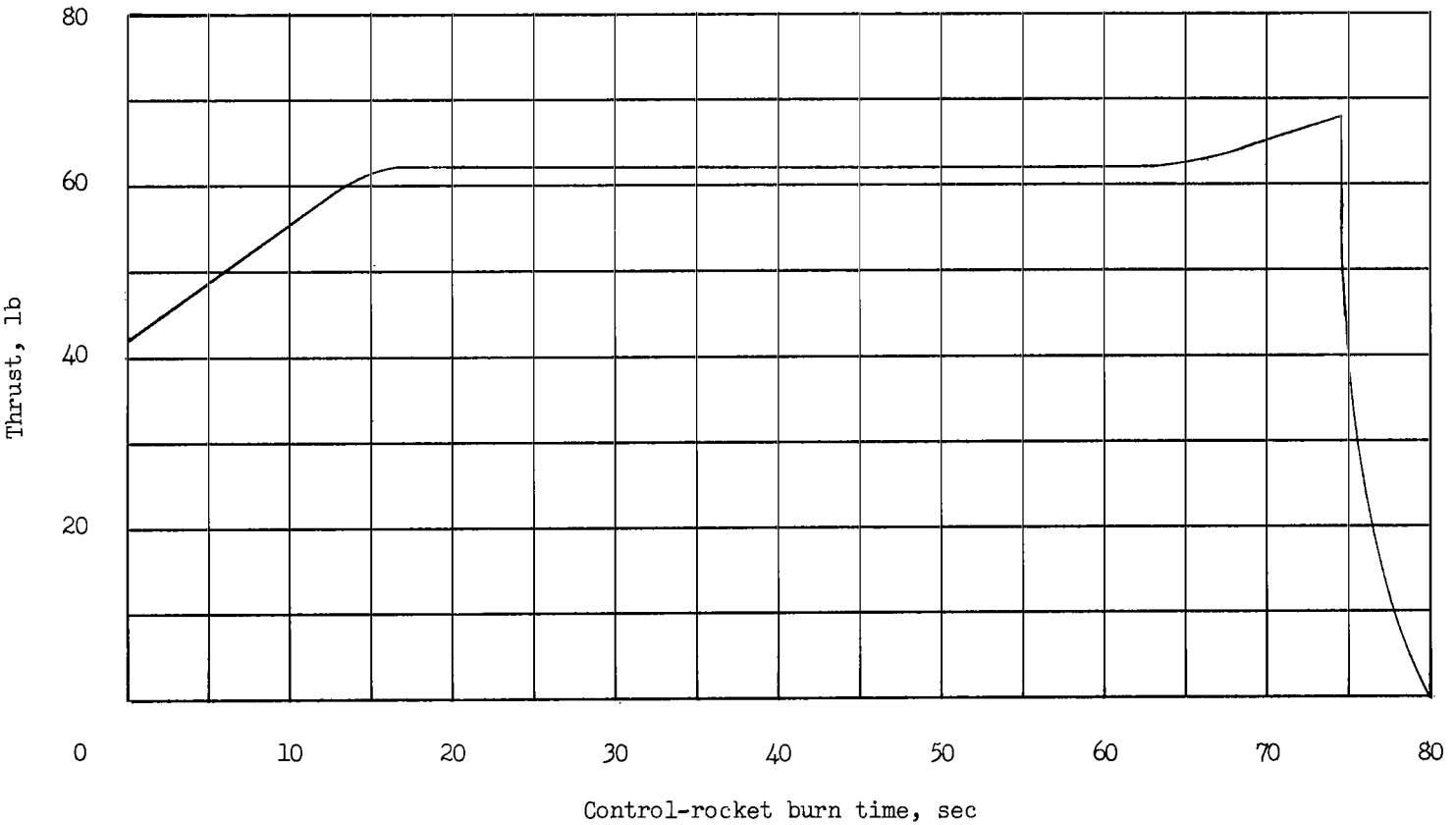

Figure 3.- Nominal thrust time history for one control rocket.

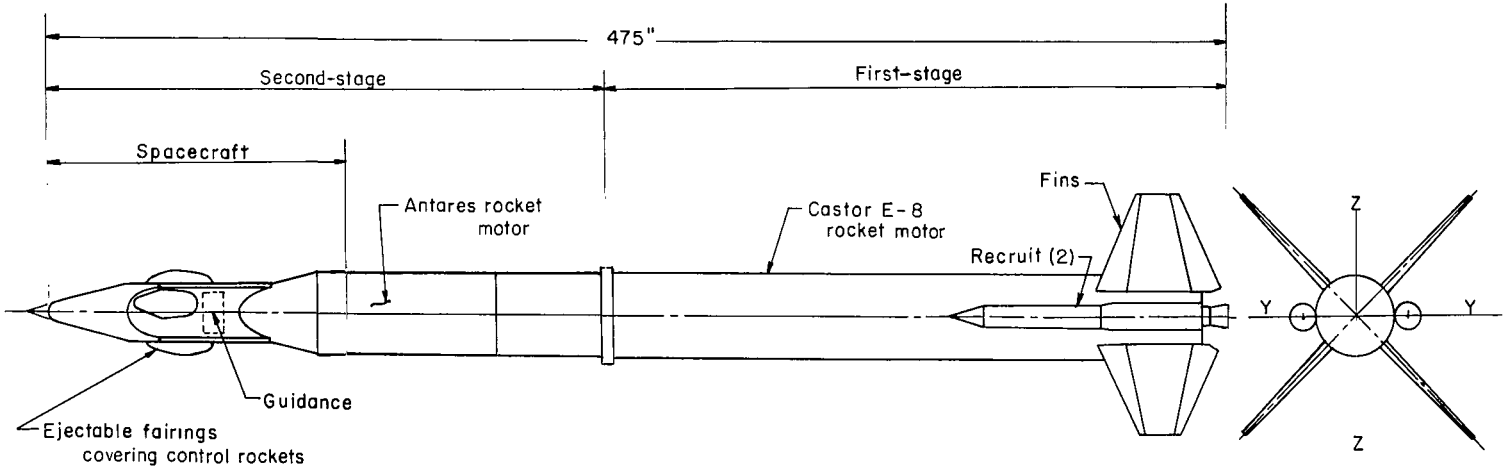

Figure 4.- General configuration of research vehicle.

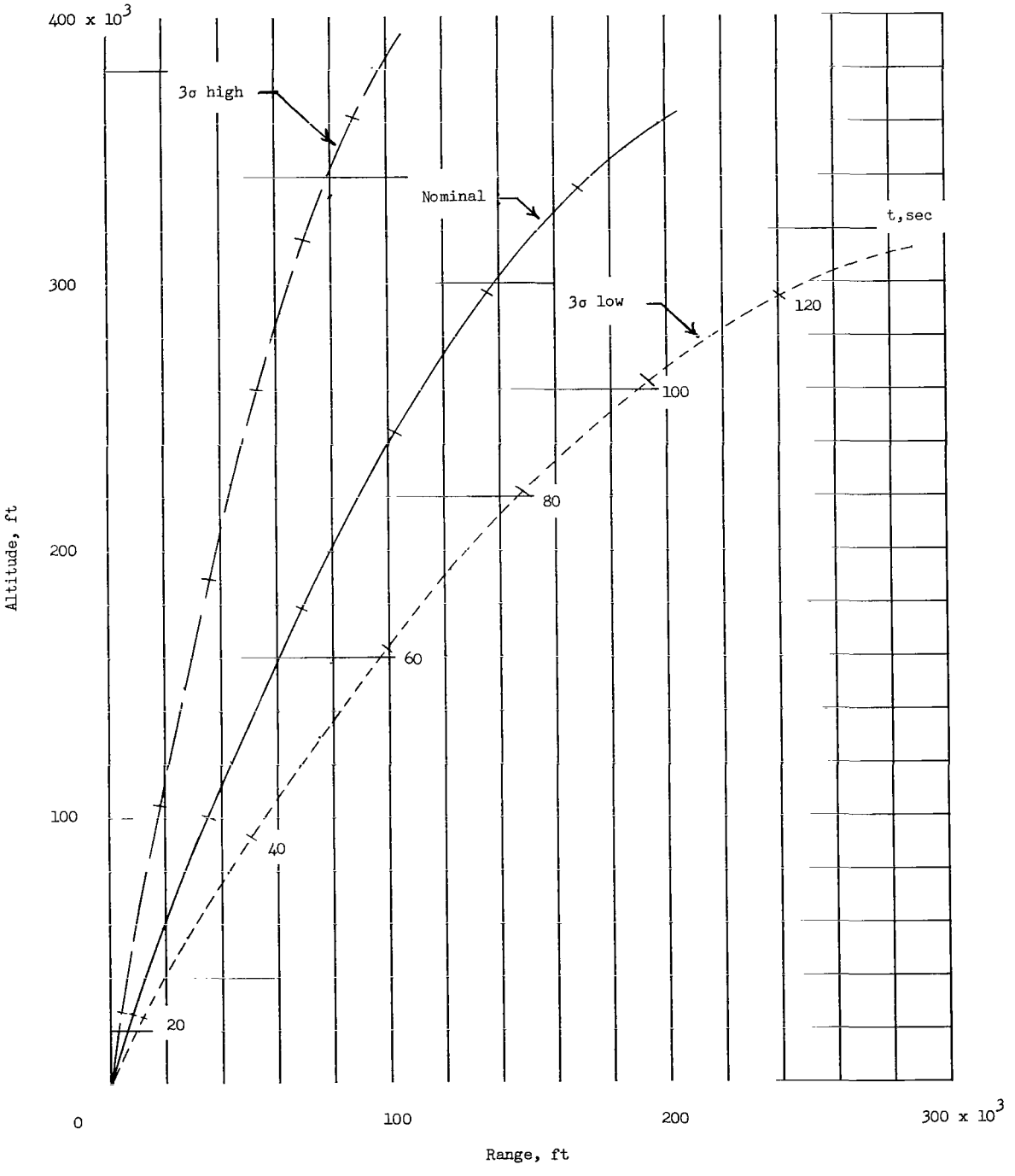

(a) Trajectory in space.

Figure 5.- Research-vehicle first-stage performance parameters.

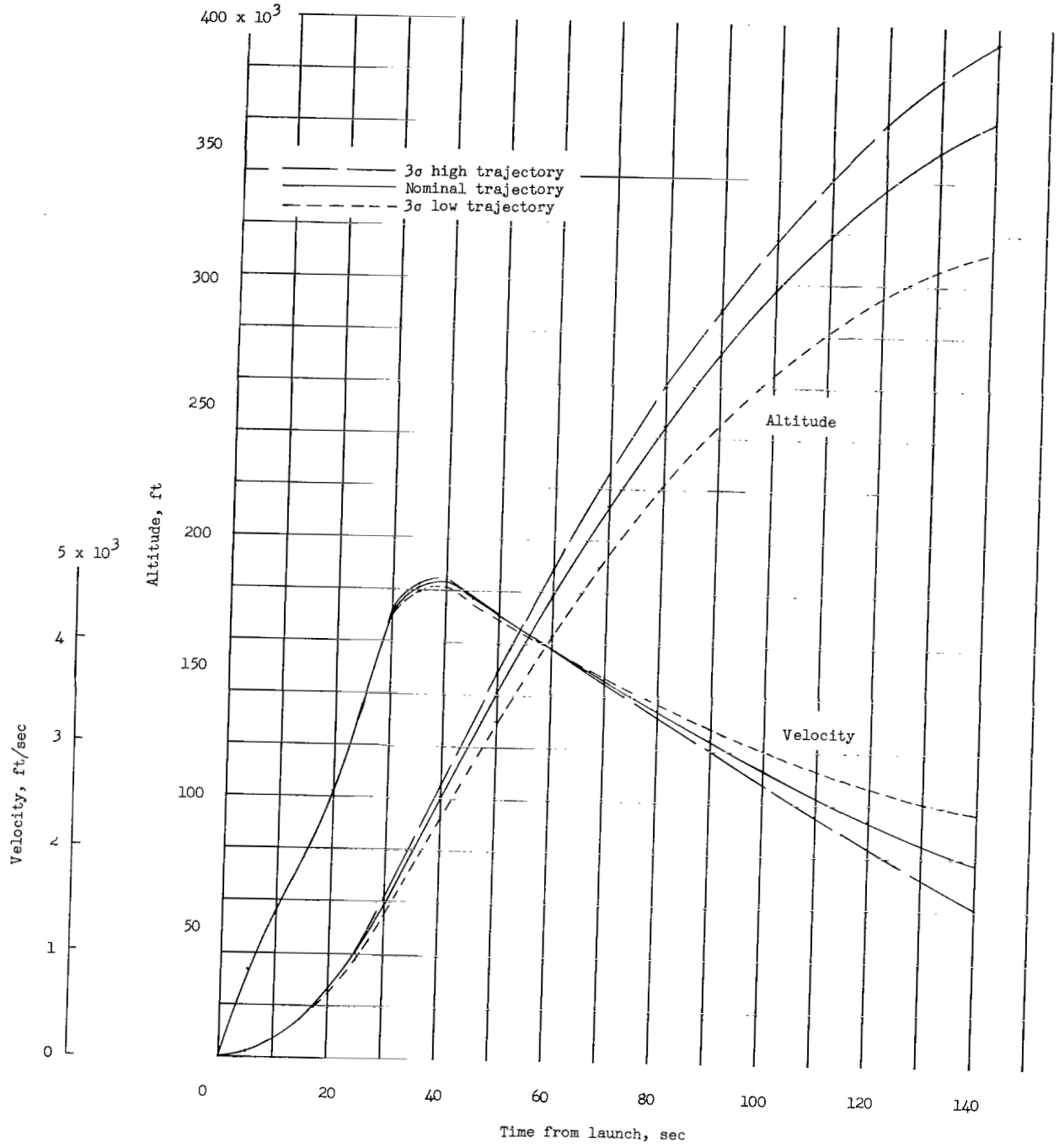

(b) Variation of velocity and altitude with time.

Figure 5.- Concluded.

see errata

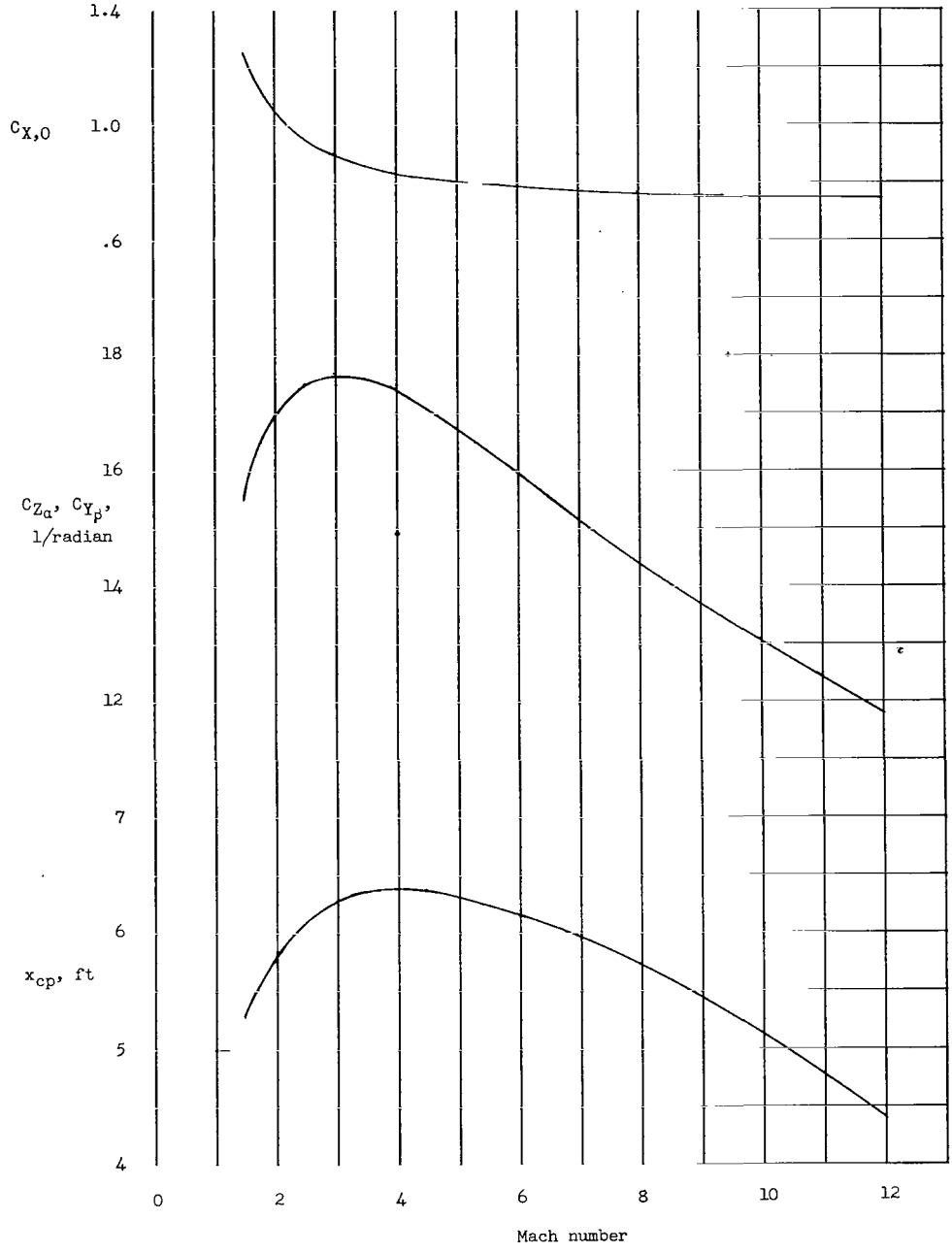

(a) Variation of $C_{X,0}$, C_{Z_α}, C_{Y_β}, and x_{cp} with Mach number.

Figure 6.- Research-vehicle second-stage aerodynamic and physical characteristics. Reference area of 1 square foot.

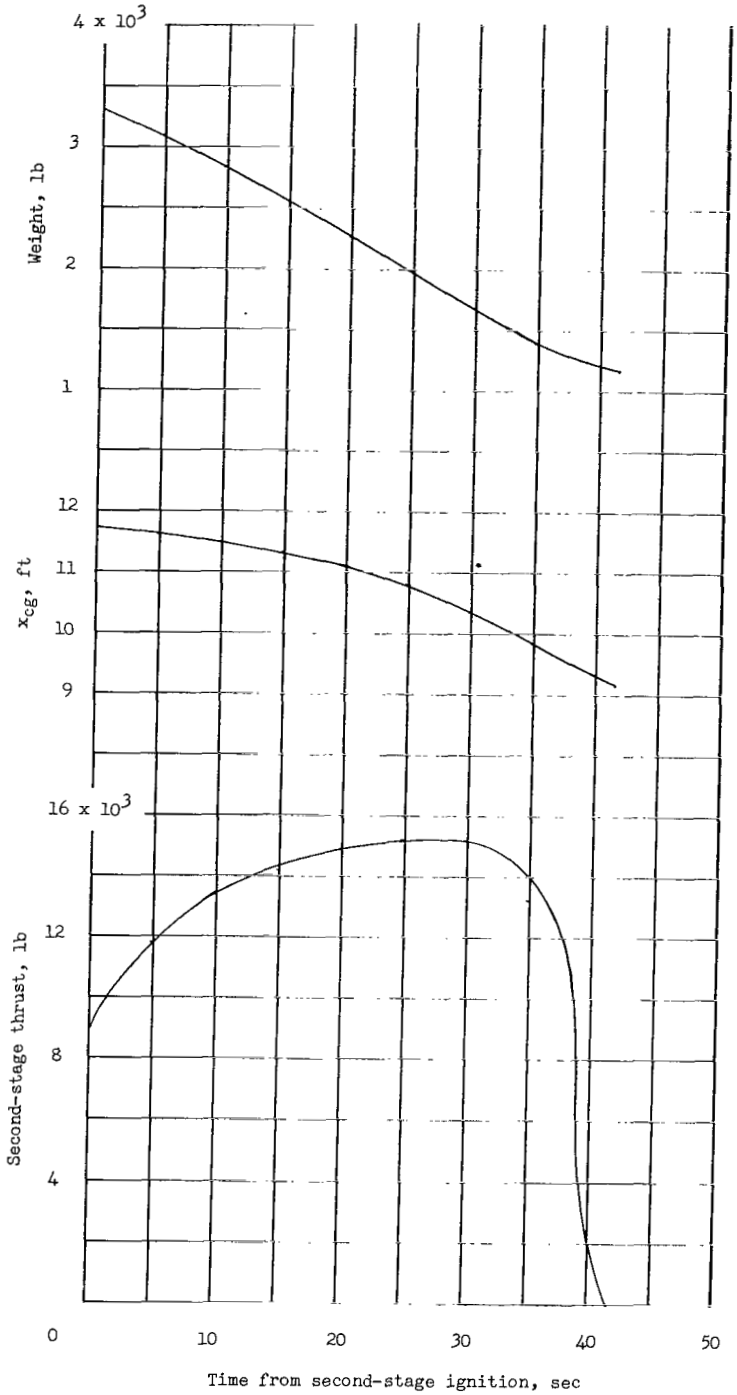

(b) Variation of second-stage thrust, x_{cg}, and weight with time.

Figure 6.- Continued.

see errata

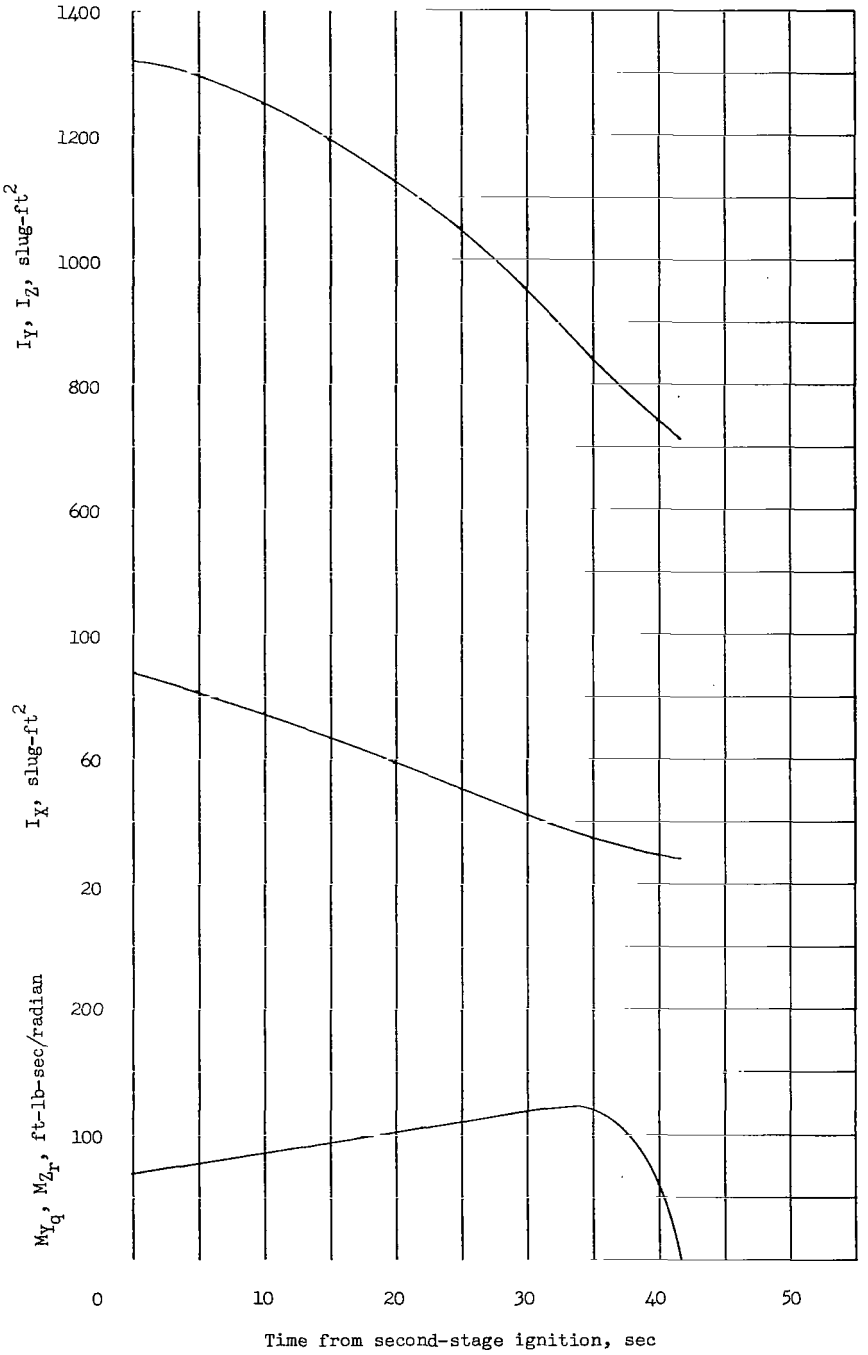

(c) Variation of M_{Y_q}, M_{Z_r}, I_X, I_Y, and I_Z with time.

Figure 6.- Concluded.

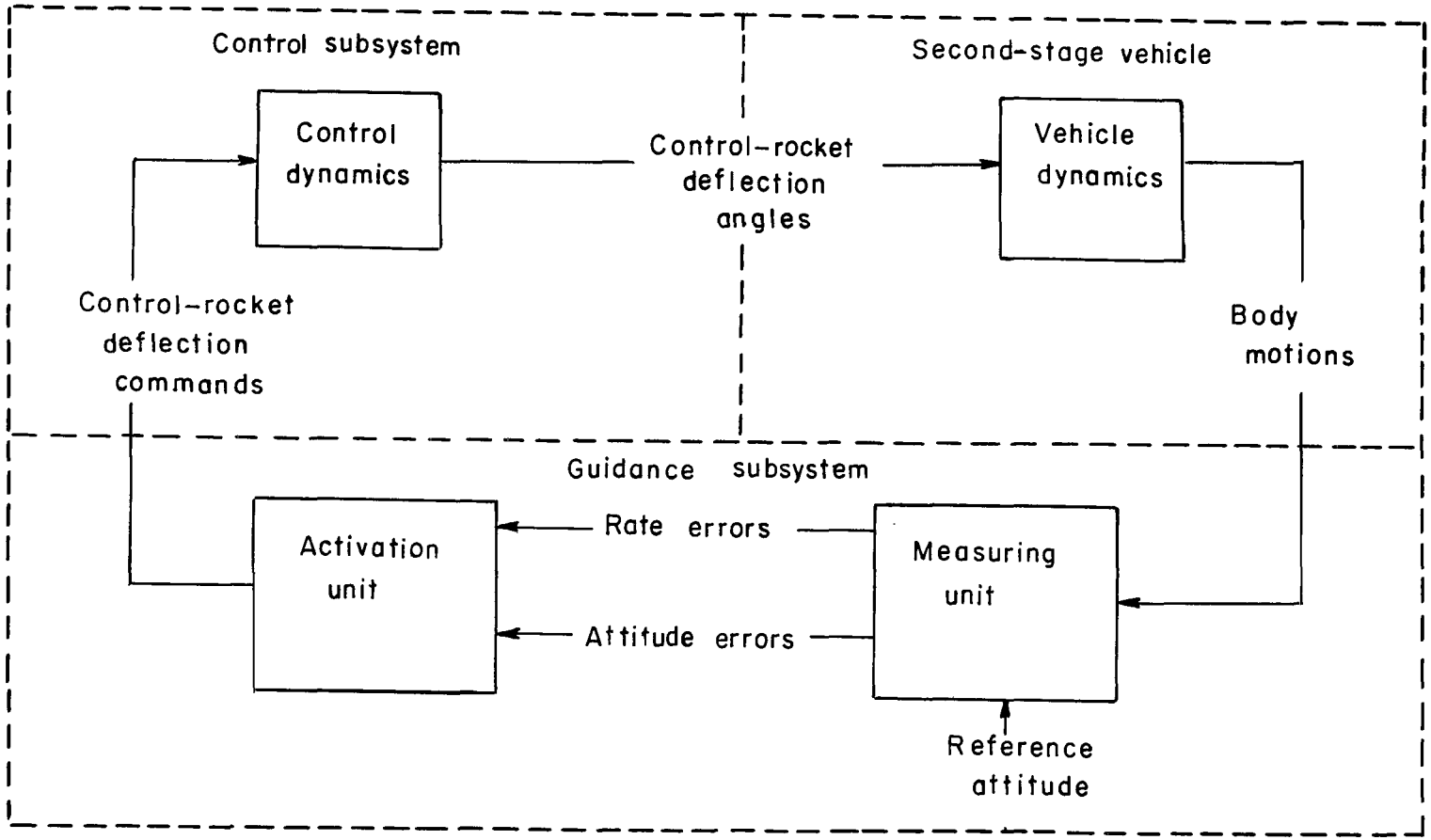

Figure 7.- Block diagram of major elements of second-stage system.

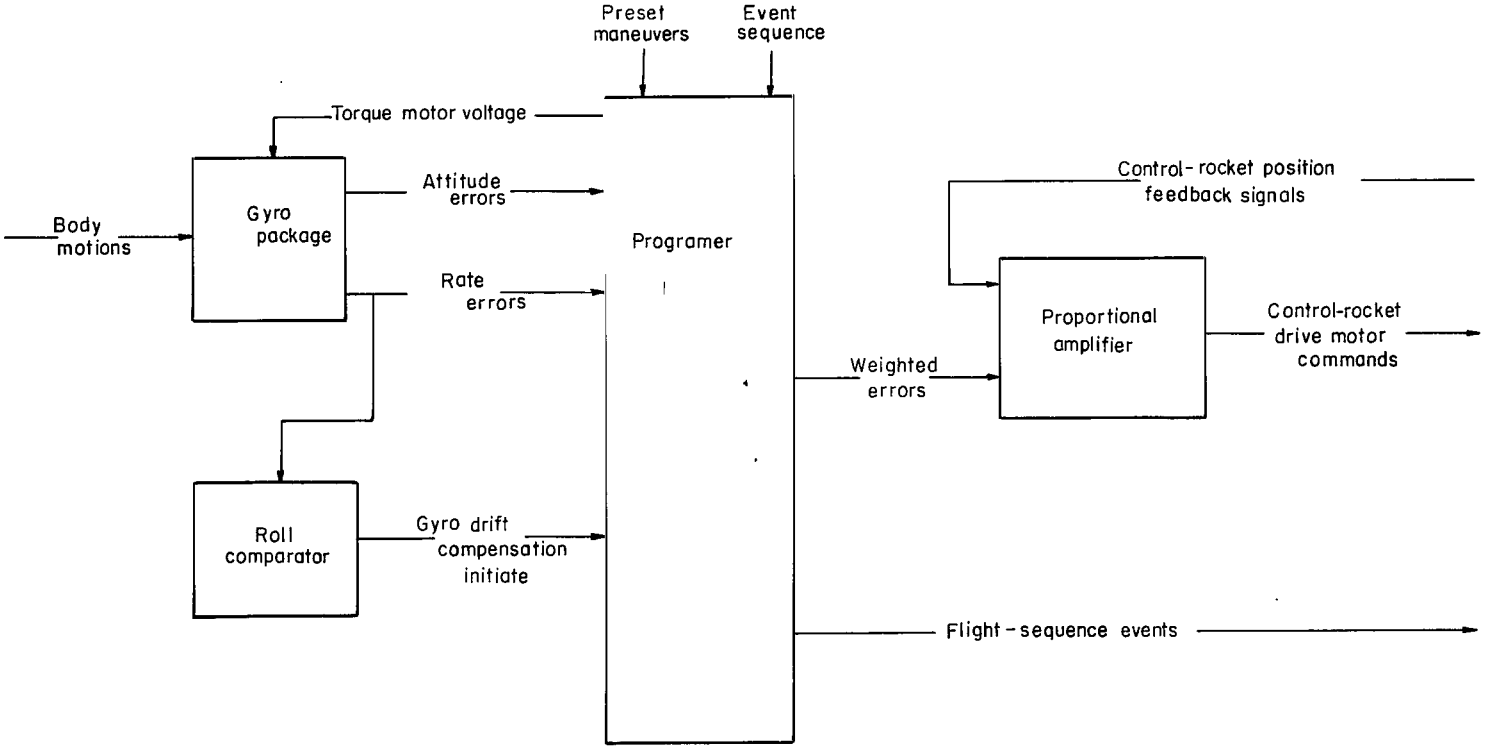

Figure 8.- Guidance subsystem functional diagram.

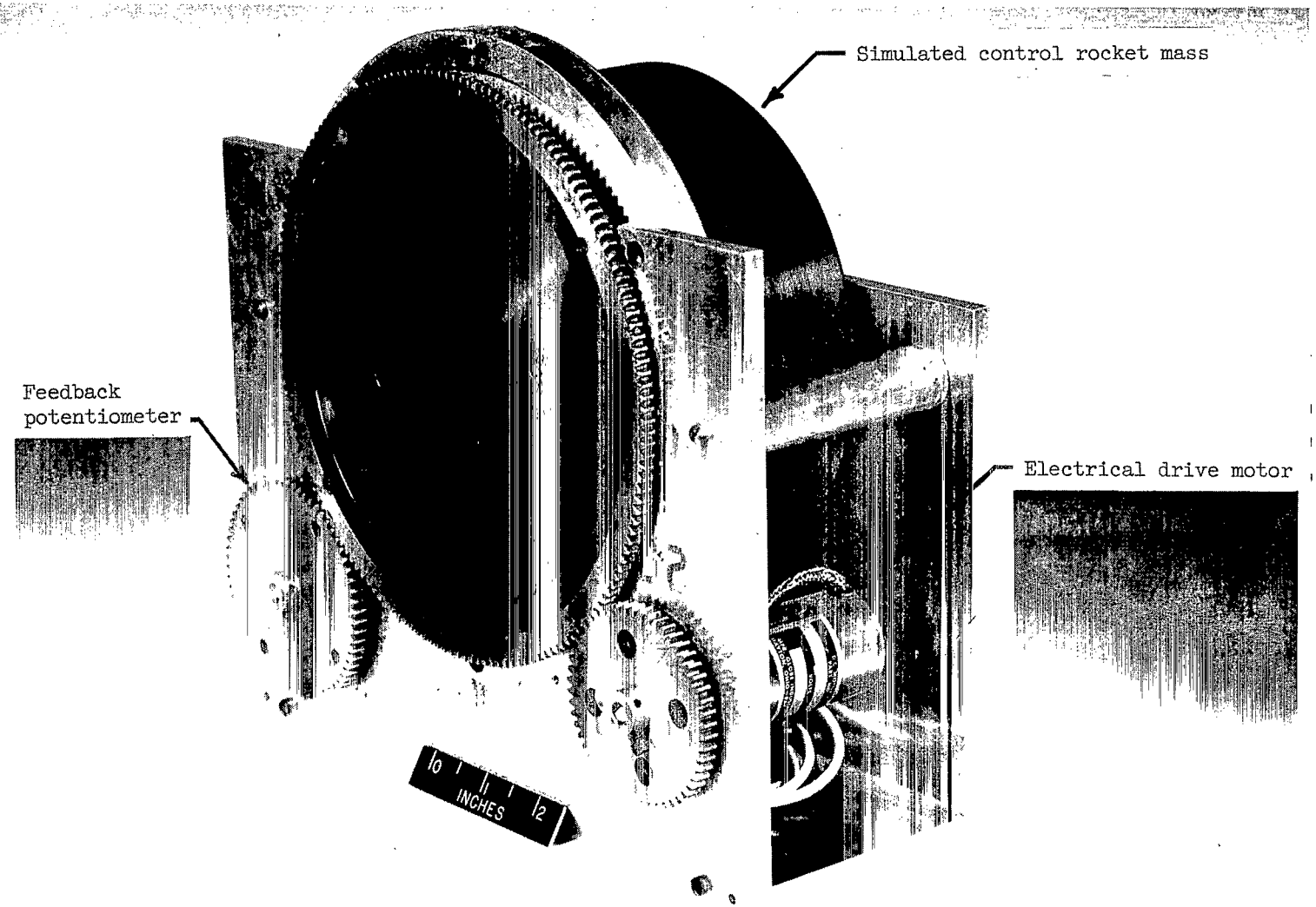

Figure 9.- Dynamic model of one loop of control system. L-64-2417.1

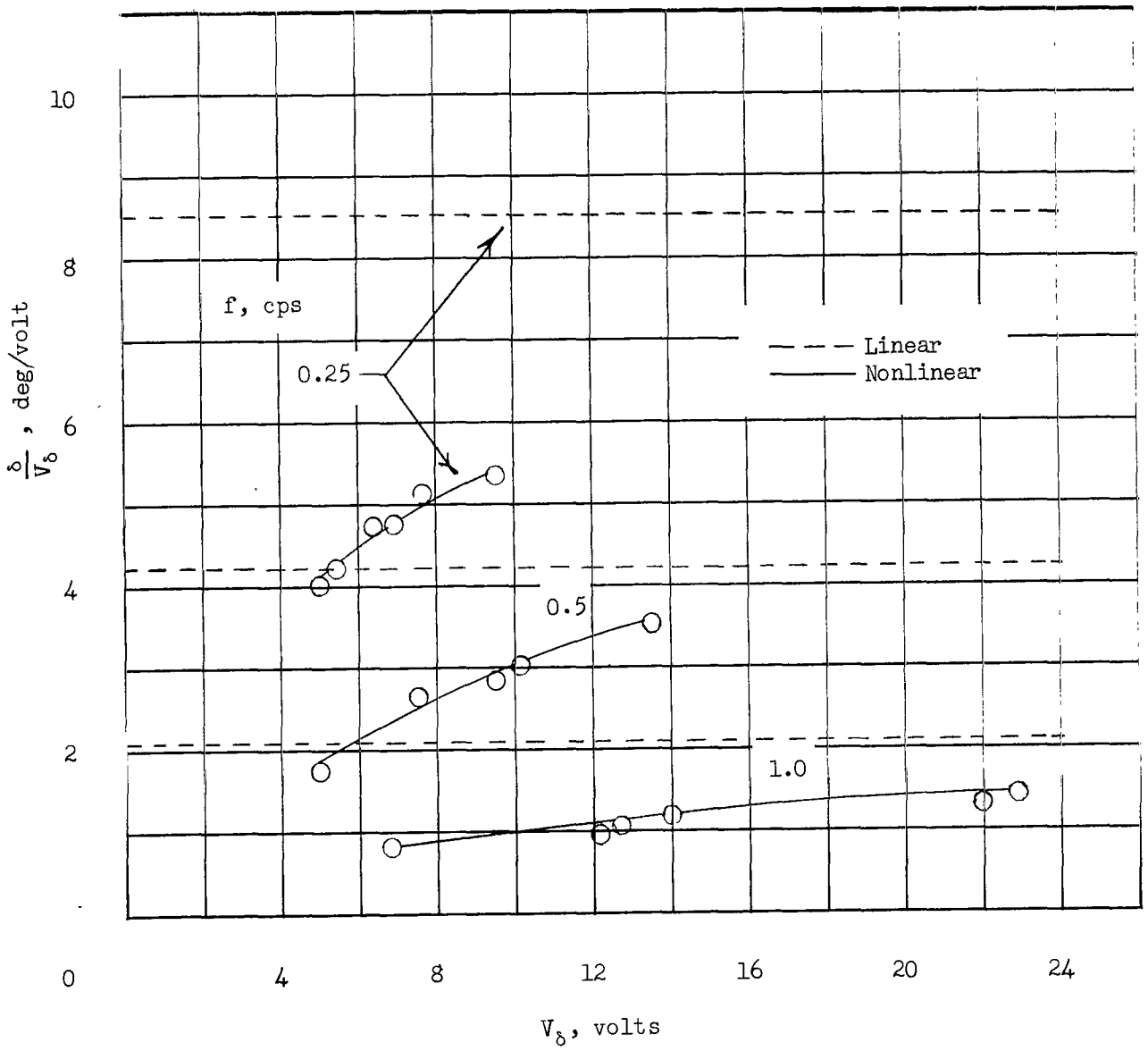

Figure 10.- Variation of amplitude ratio with input voltage and frequency.

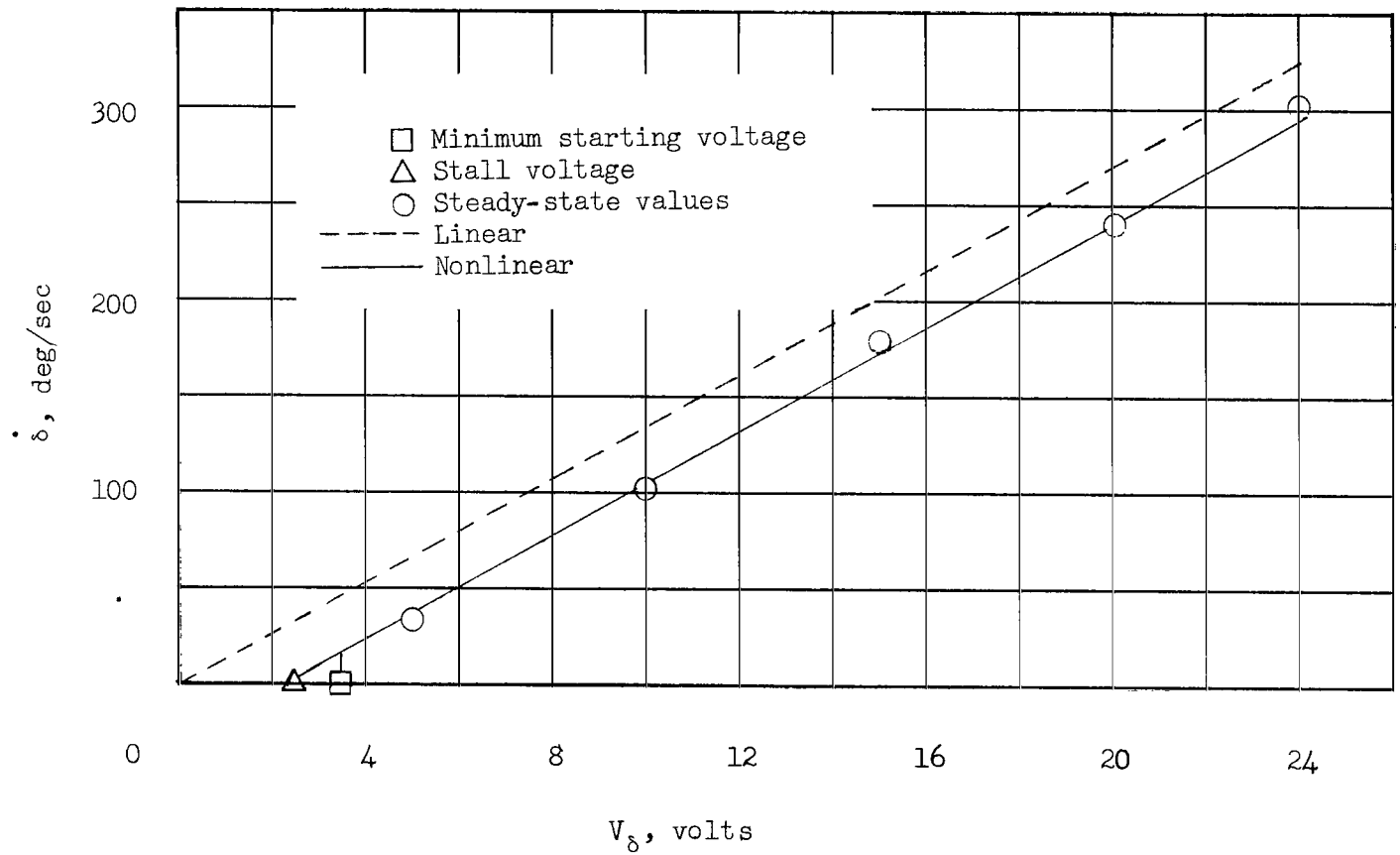

Figure 11.- Variation of control-rocket deflection rate with input voltage.

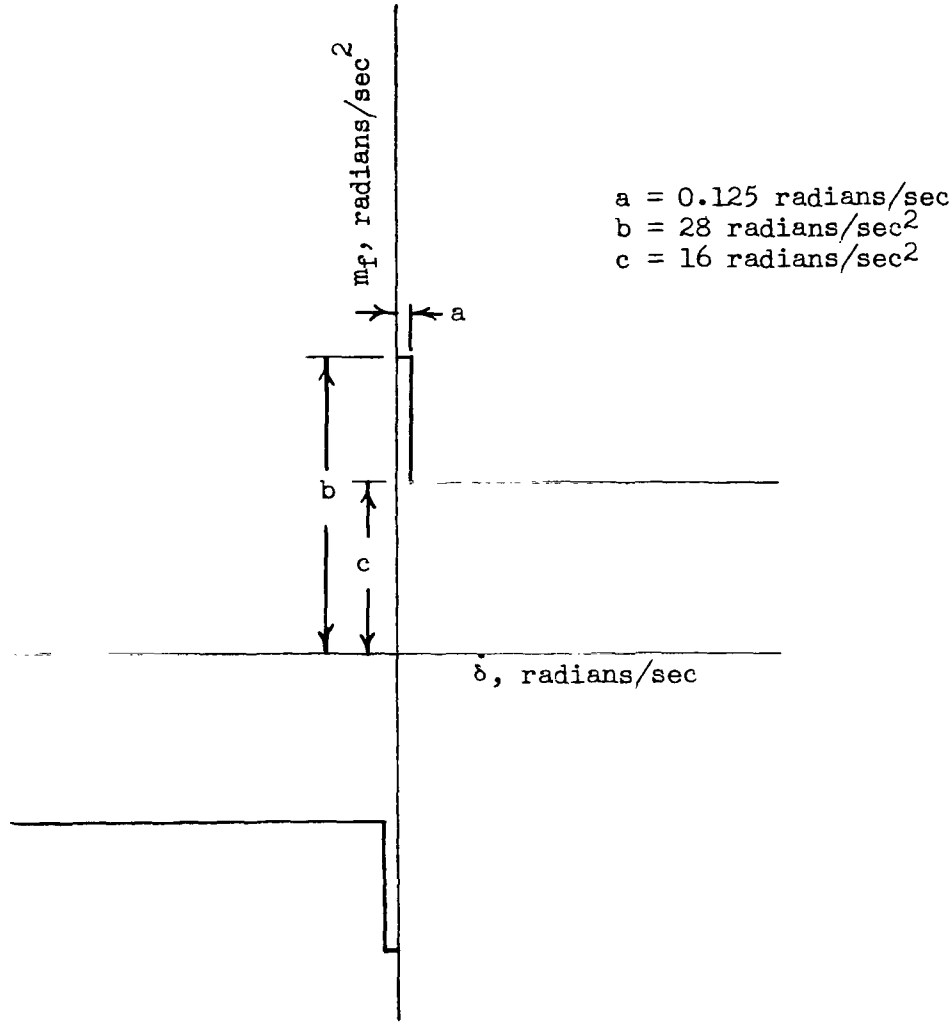

Figure 12.- Control subsystem frictional nonlinearities.

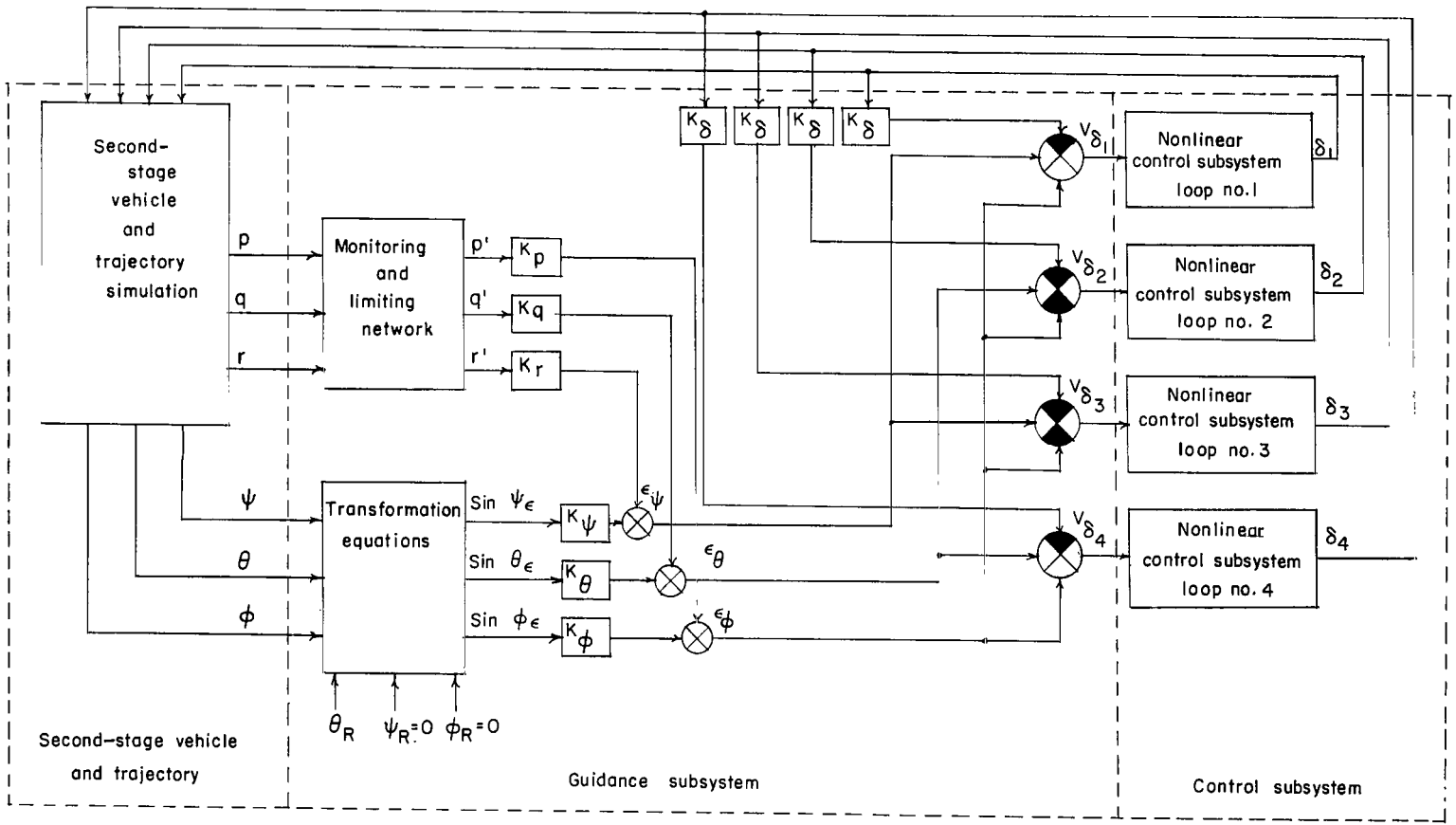

Figure 13.- Second-stage system simulation.

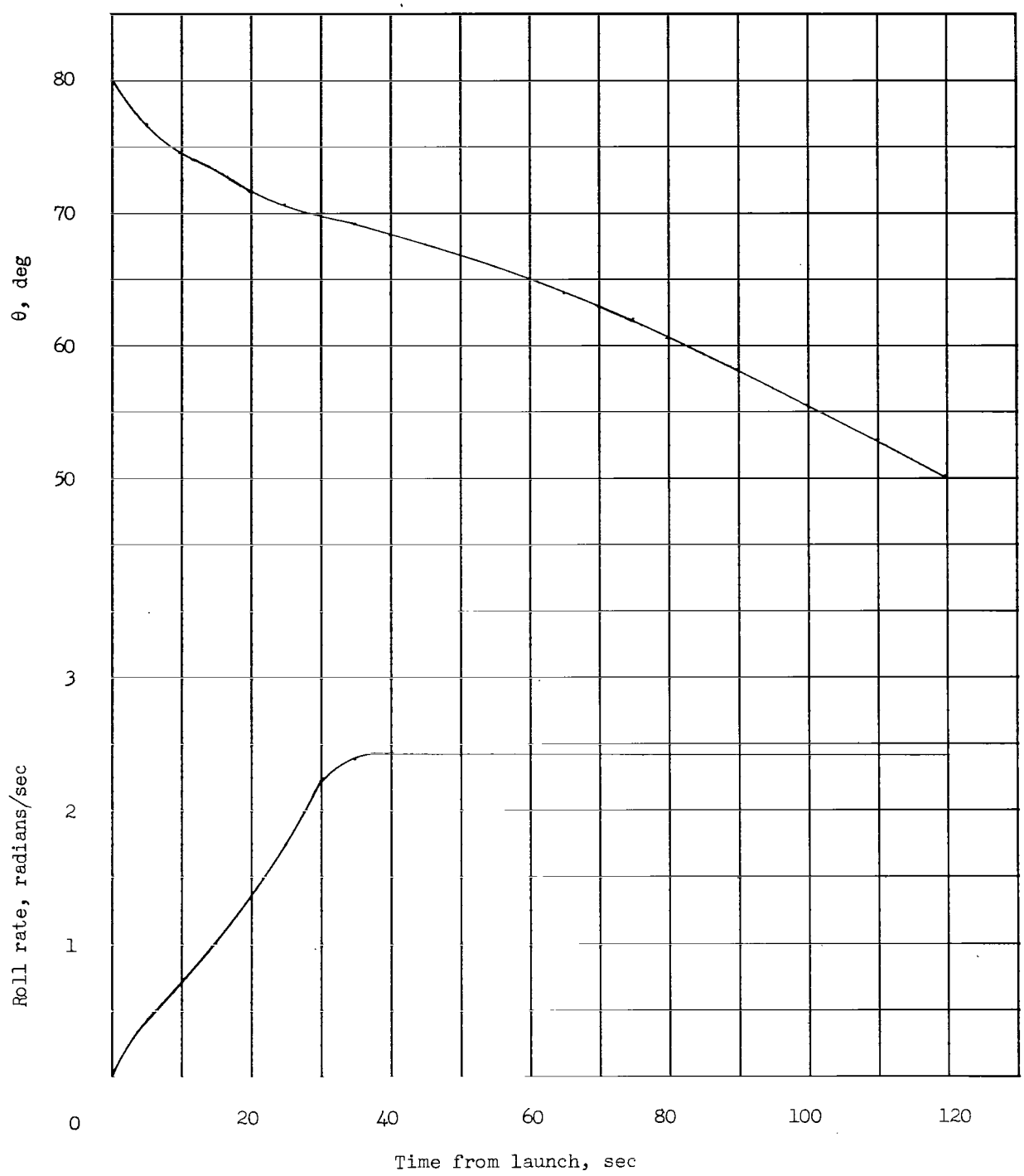

Figure 14.- Variation of first-stage 3σ roll rate and nominal pitch attitude with time.

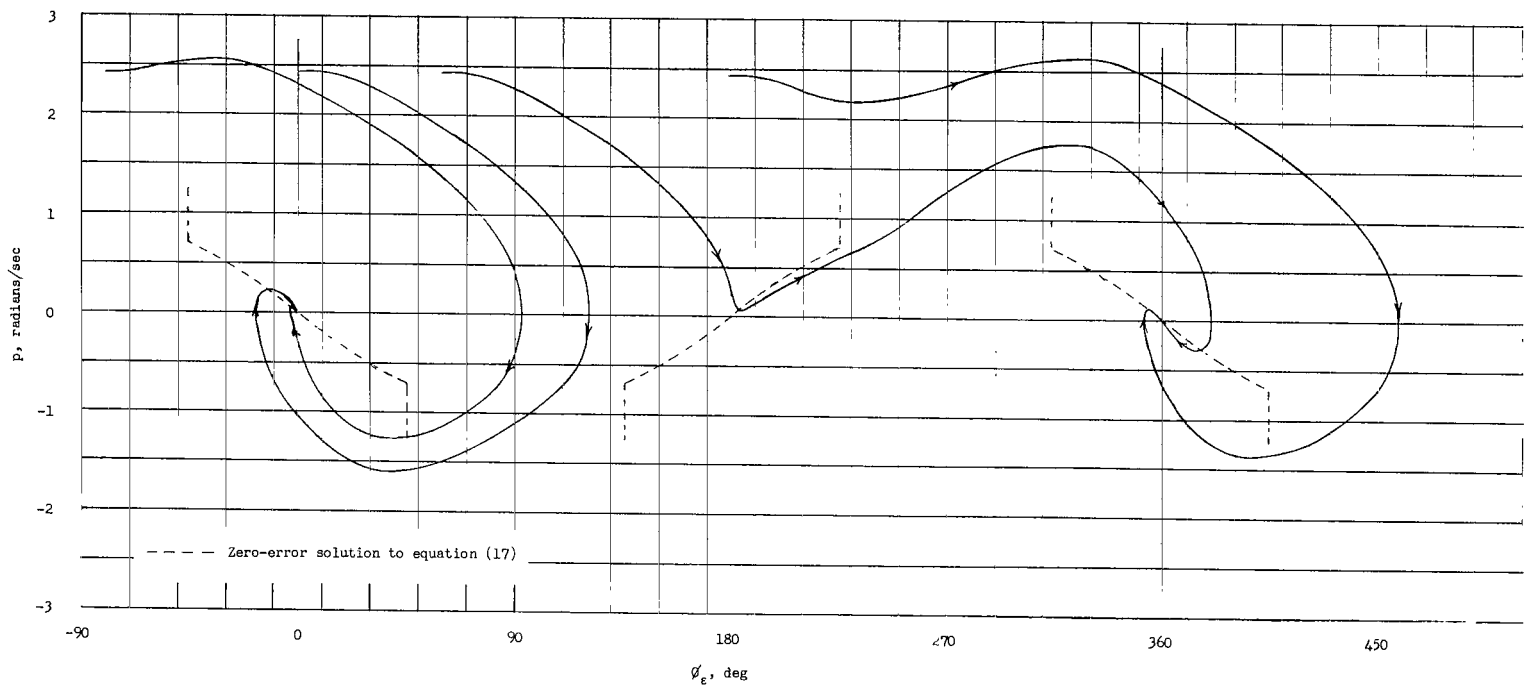

(a) $K\phi$ = 200 volts/radian and K_p = 200 volts/radian/sec.

Figure 15.- Roll-phase plane trajectories.

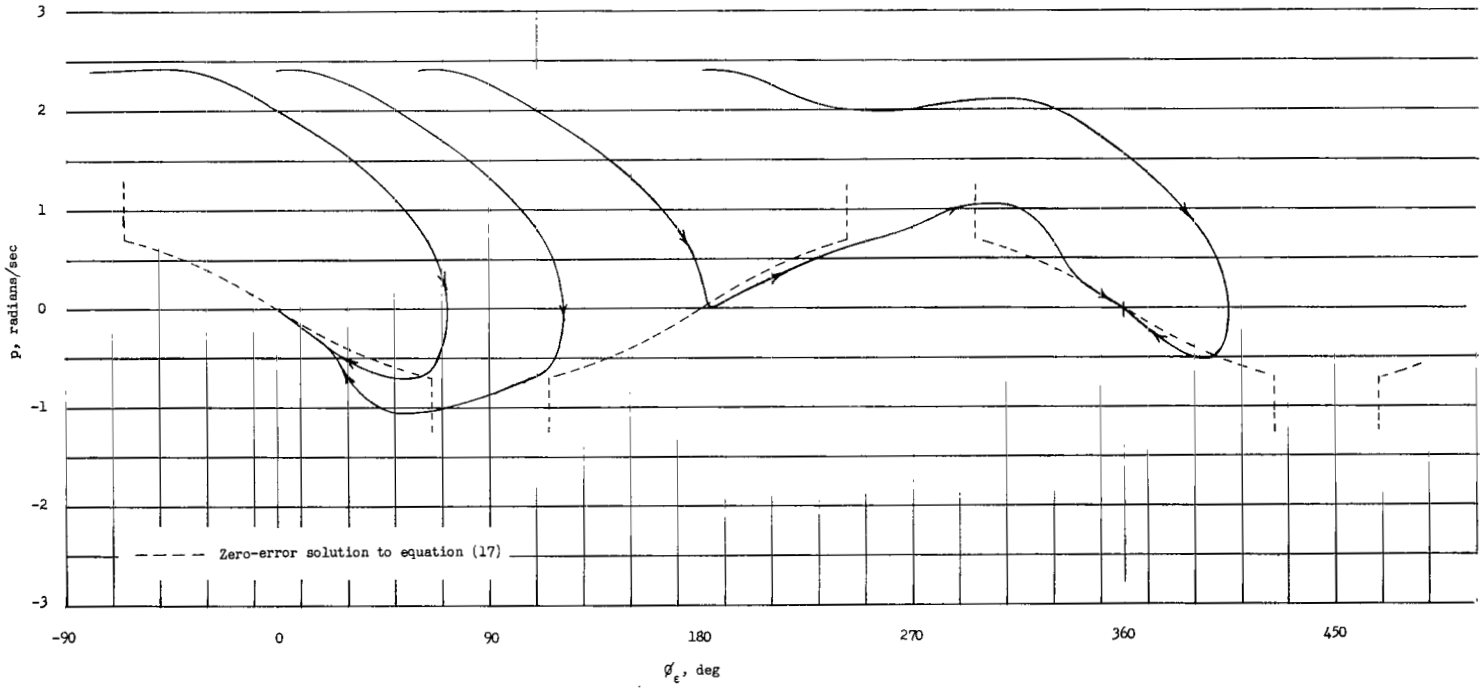

(b) K_ϕ = 200 volts/radian and K_p = 250 volts/radian/sec.

Figure 15.- Continued.

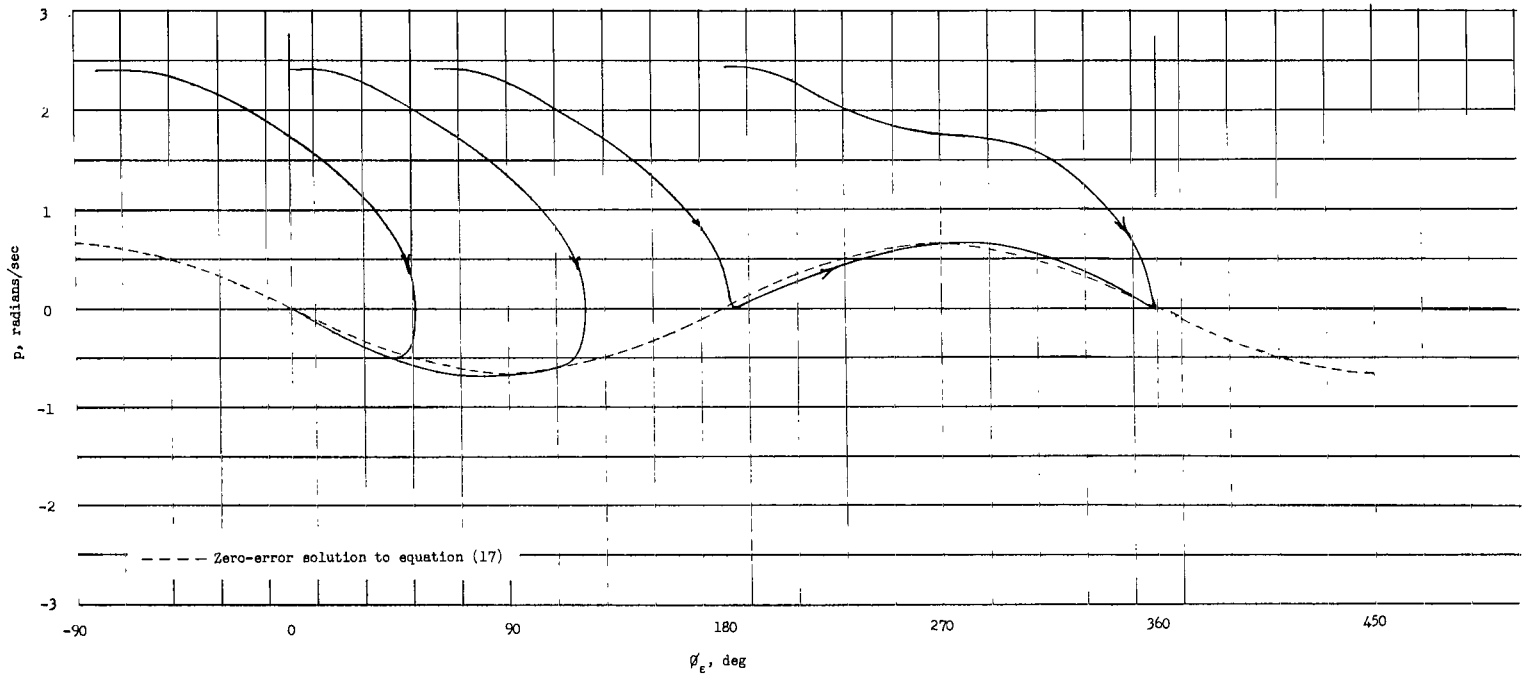

(c) K_ϕ = 200 volts/radian and K_p = 300 volts/radian/sec.

Figure 15.- Continued.

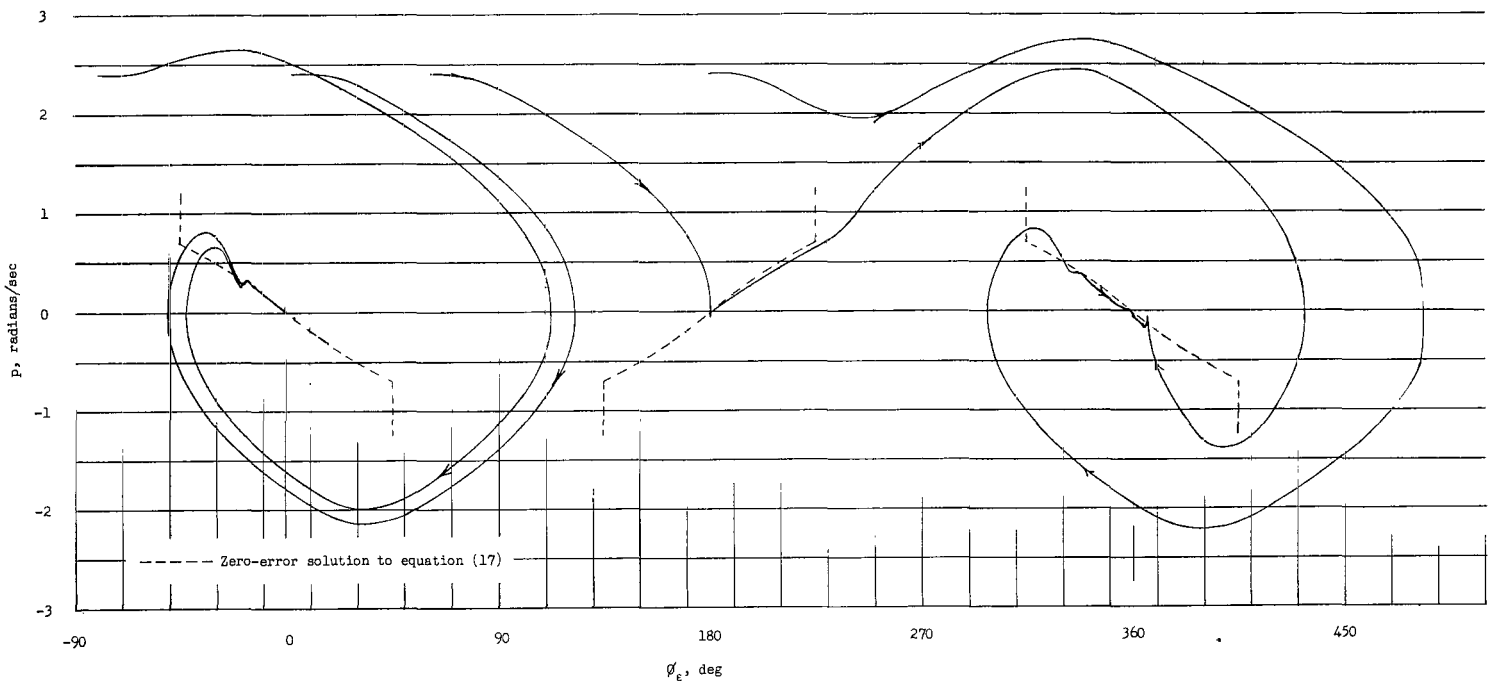

(d) K_ϕ = 600 volts/radian and K_p = 600 volts/radian/sec.

Figure 15.- Continued.

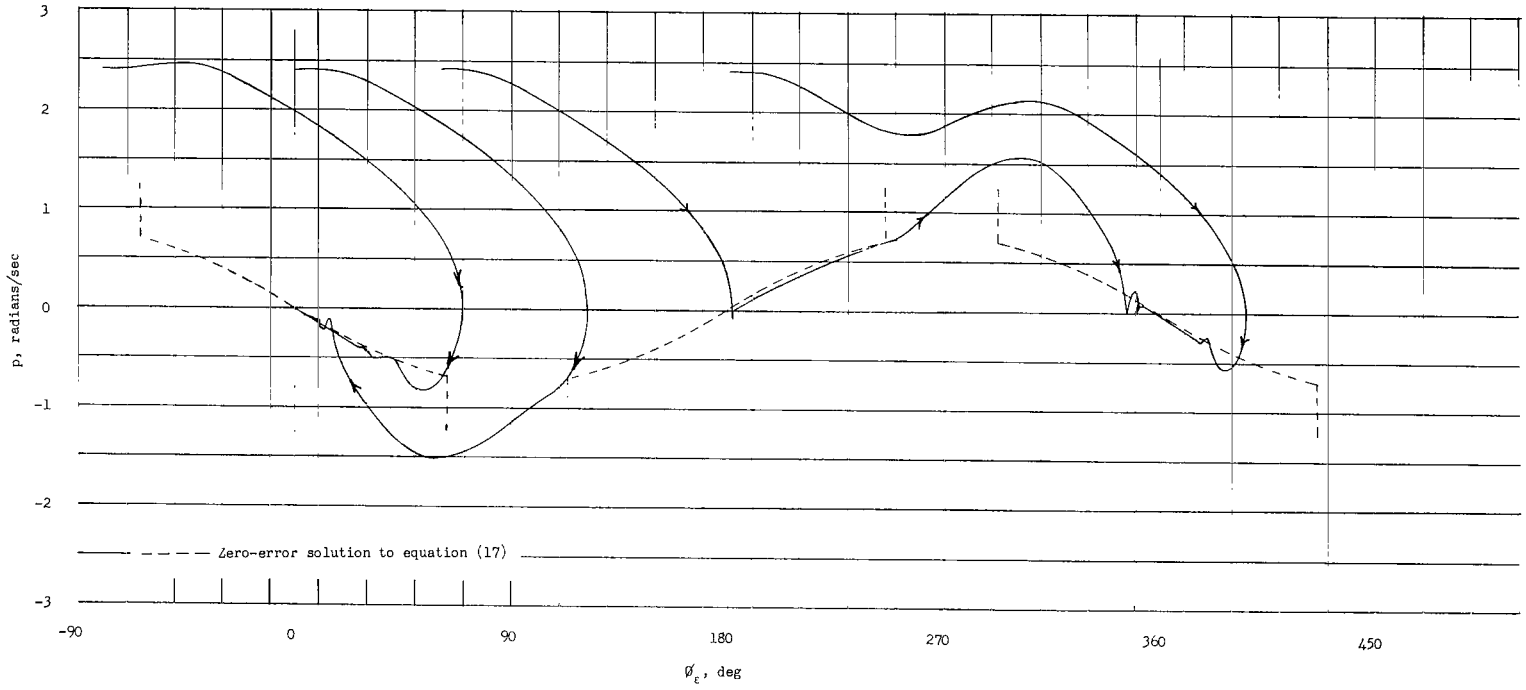

(e) K_ϕ = 600 volts/radian and K_p = 750 volts/radian/sec.

Figure 15.- Continued.

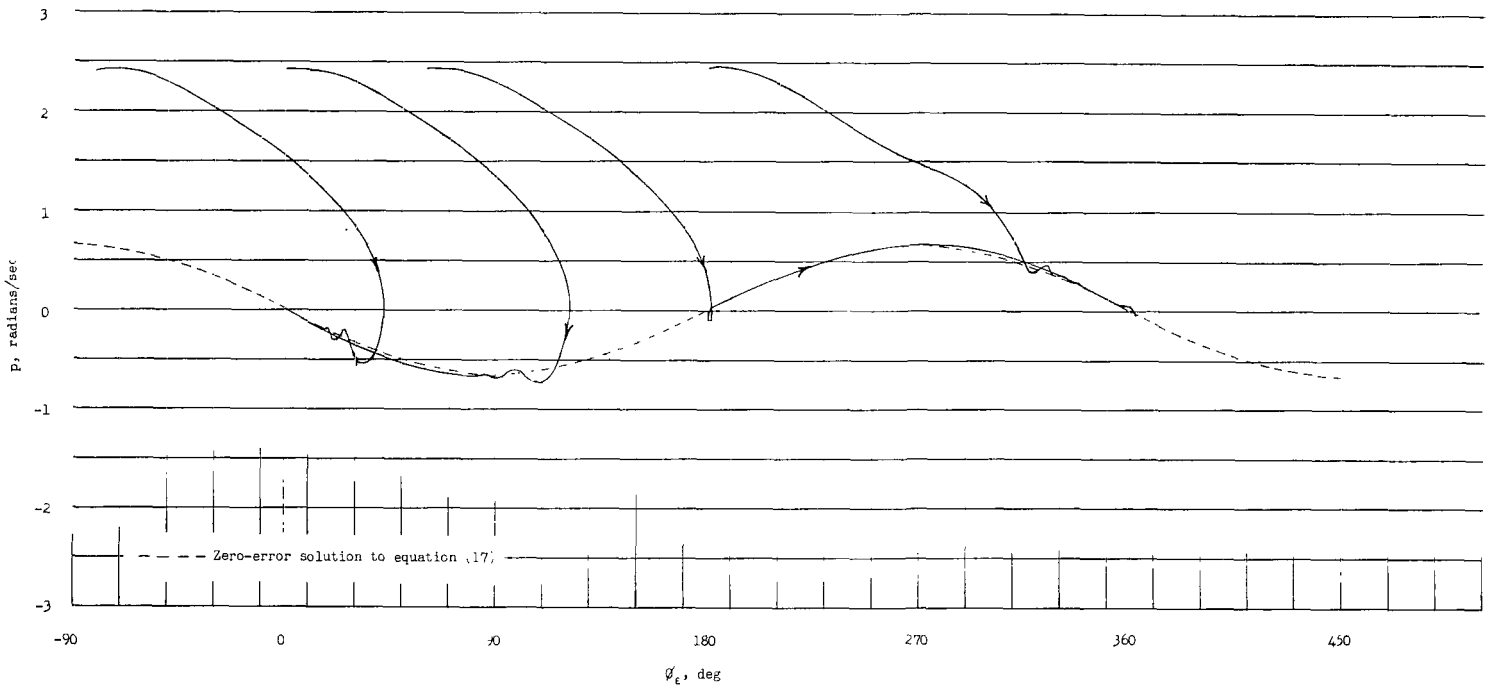

(f) K_ϕ = 600 volts/radian and K_p = 900 volts/radian/sec.

Figure 15.- Concluded.

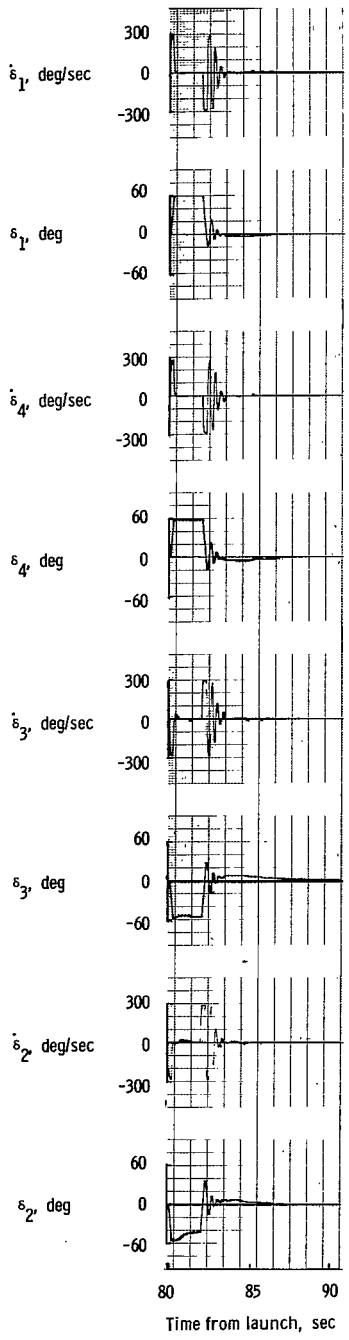

(a) K_ϕ = 600 volts/radian and K_p = 900 volts/radian/sec.

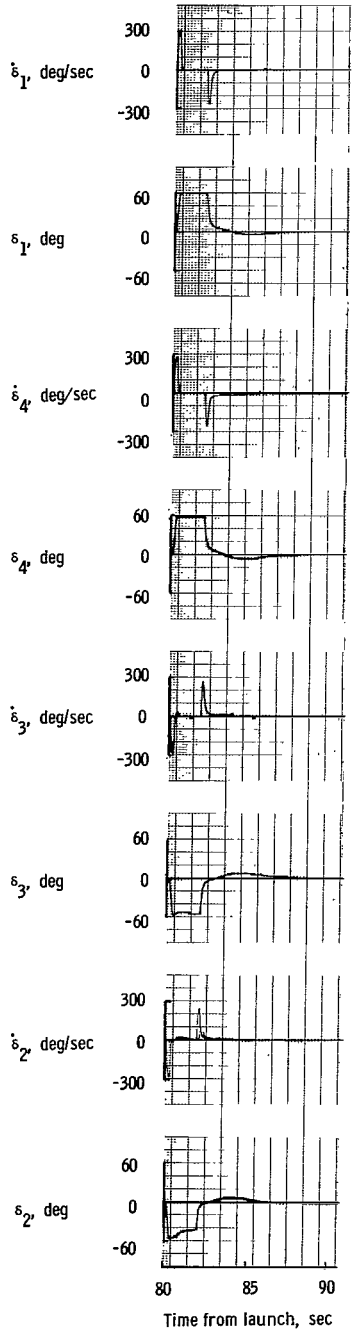

(b) K_ϕ = 200 volts/radian and K_p = 300 volts/radian/sec.

Figure 16.- Effect of roll gains on control subsystem performance.

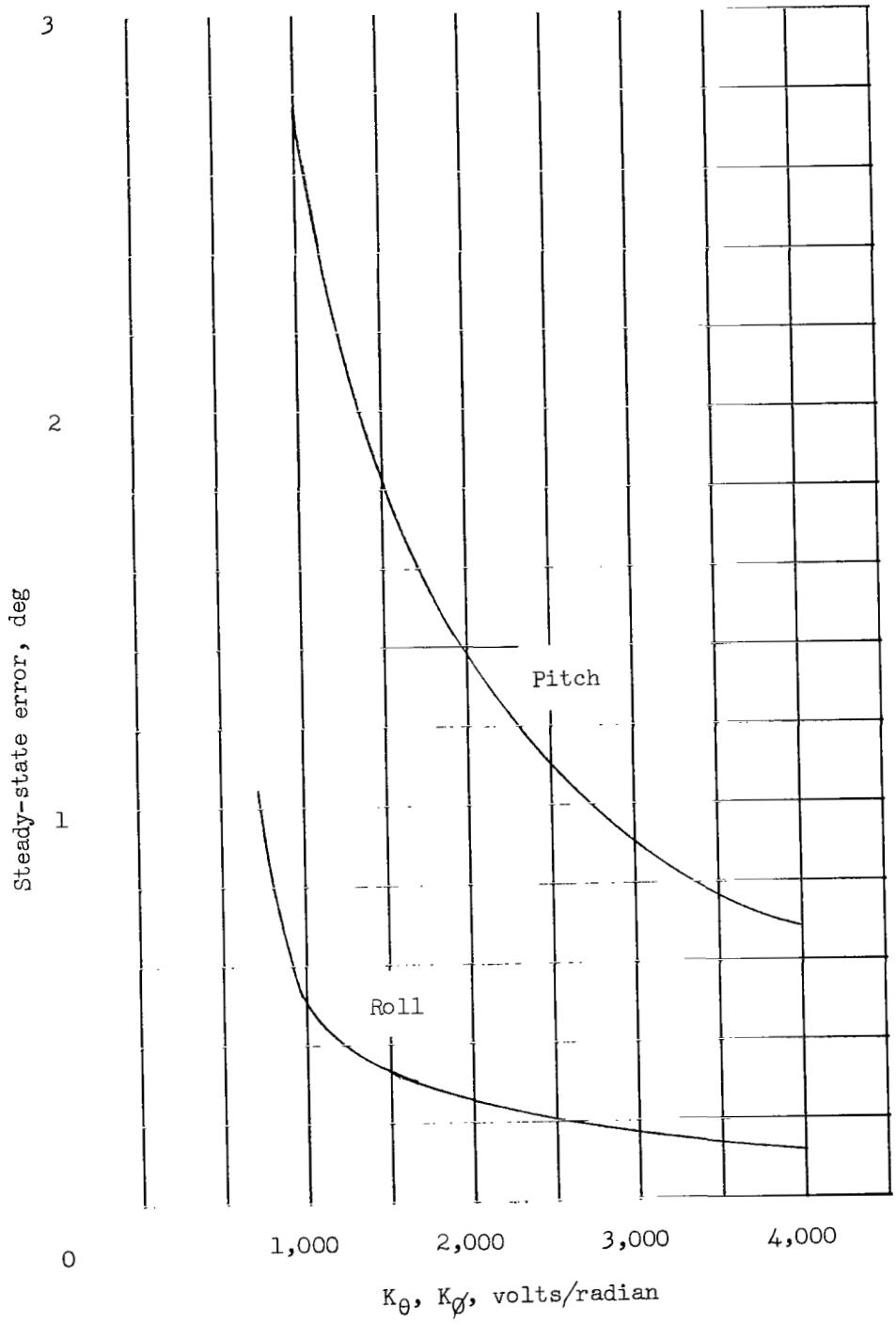

Figure 17.- Steady-state error variation with pitch- and roll-attitude gains. K_δ, 100 volts/radian; roll thrust misalinement moment, 25 ft-lb; pitch thrust misalinement moment, 250 ft-lb.

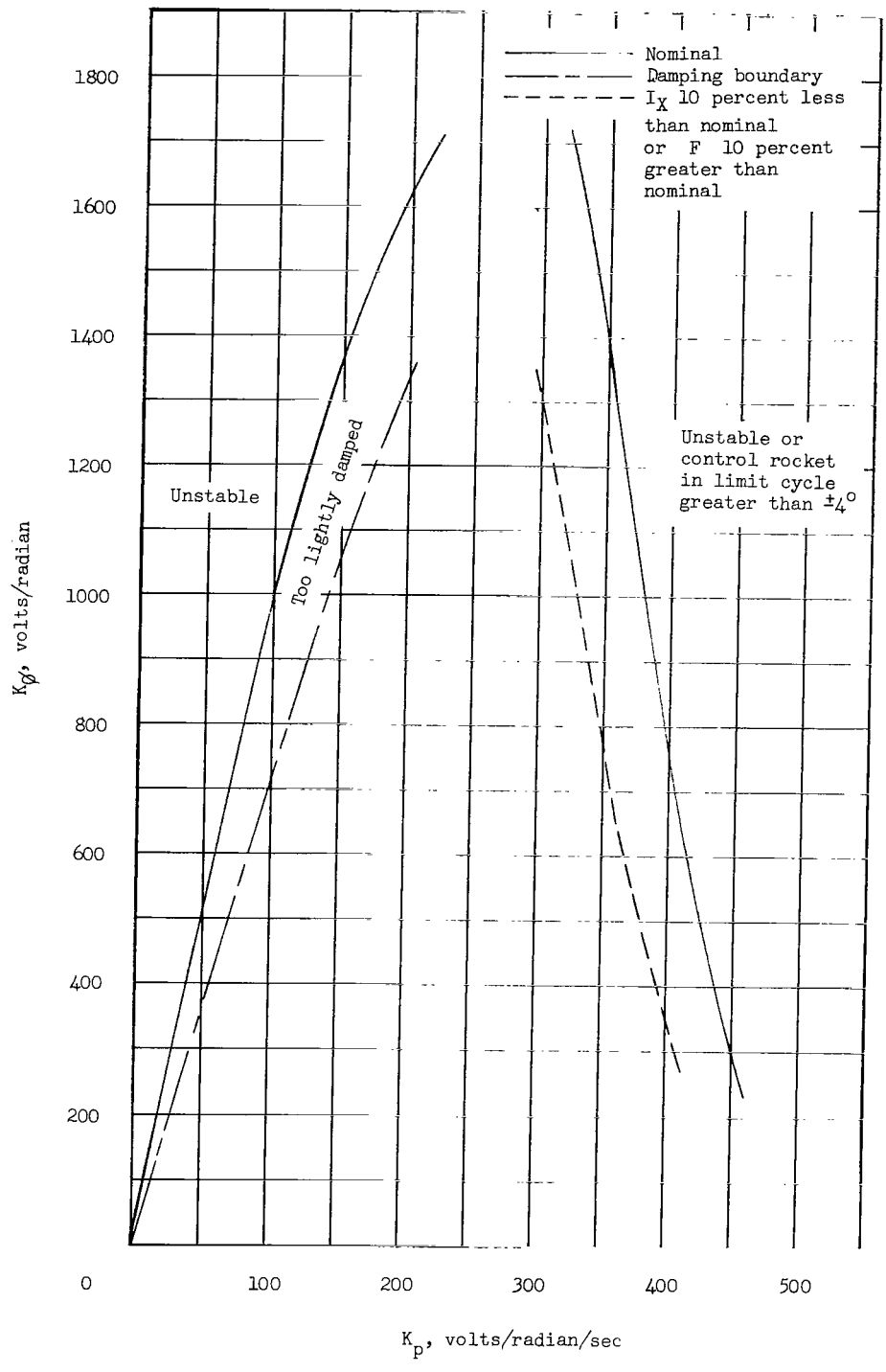

Figure 18.- Roll stability boundaries. Constant-gain parameters: $K_\theta = K_\psi$ = 2,000 volts/radian; $K_q = K_r$ = 1,300 volts/radian; K_δ = 100 volts/radian.

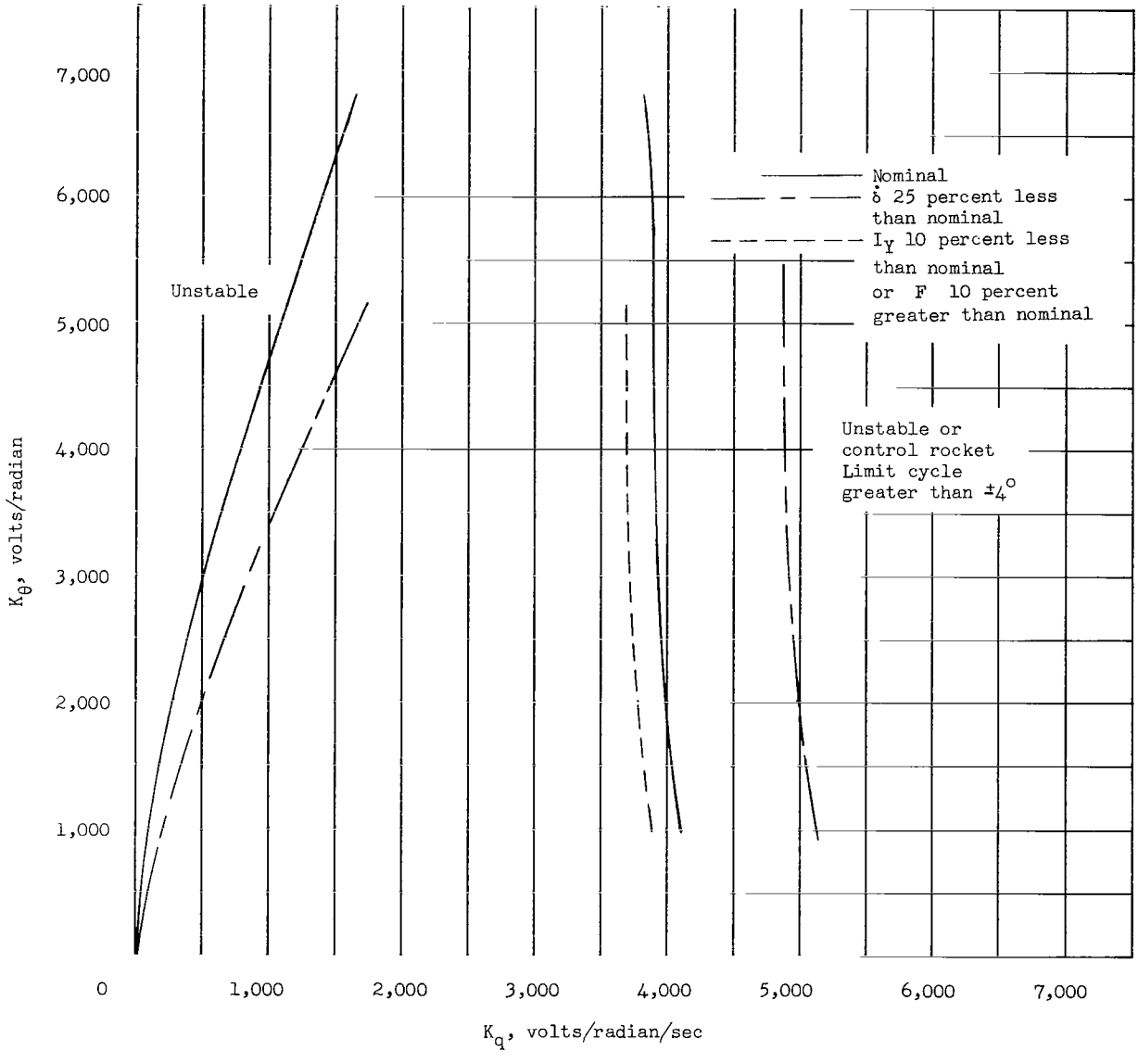

Figure 19.- Pitch stability boundaries. Constant-gain parameters: K_ϕ = 600 volts/radian; K_p = 250 volts/radian/sec; K_δ = 100 volts/radian.

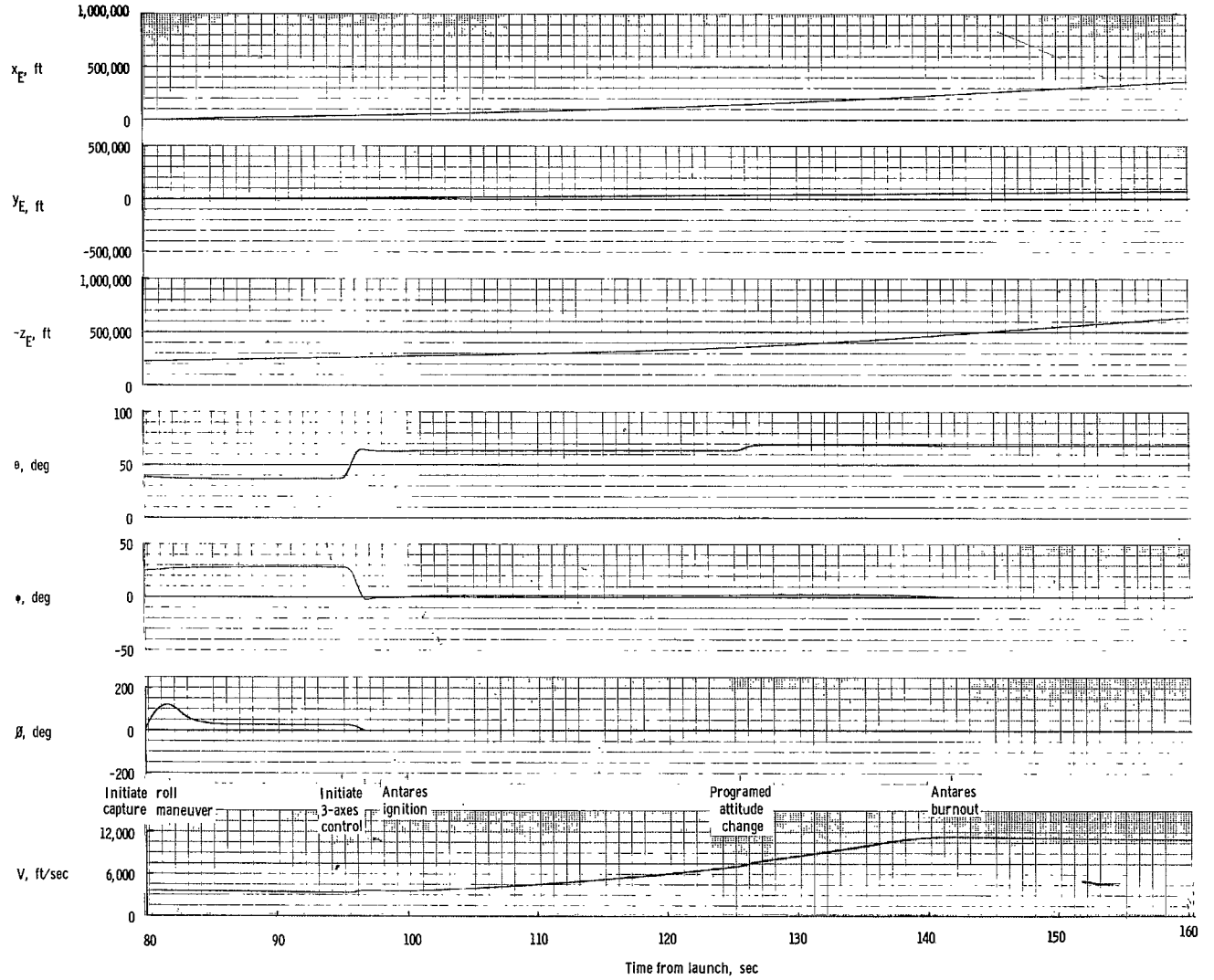

(a) Variation of x_E, y_E, $-z_E$, θ, ψ, ϕ, and V with time.

Figure 20.- Predicted research-vehicle second-stage flight time histories.

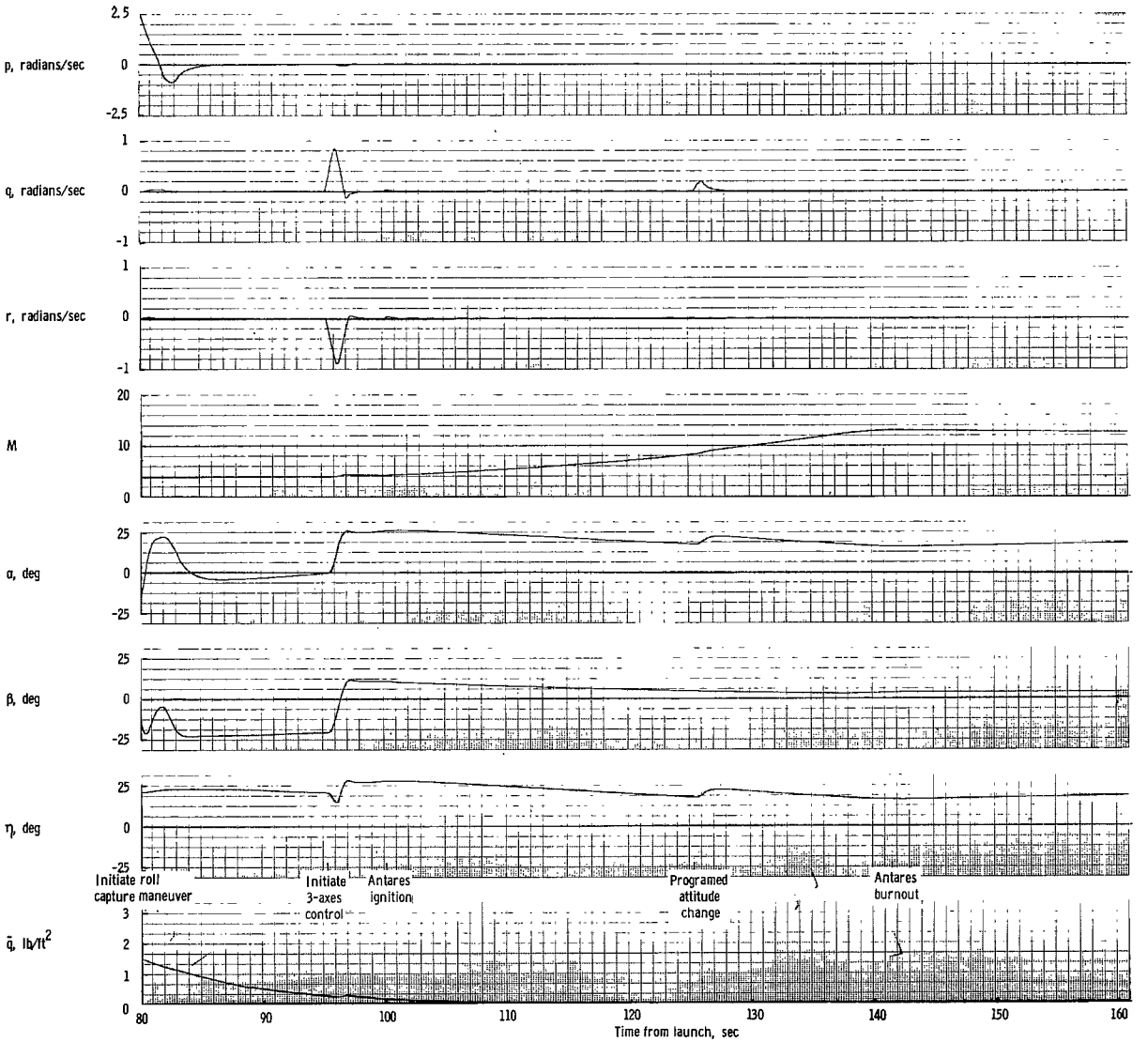

(b) Variation of p, q, r, M, α, β, η, and $\bar{q}$ with time.

Figure 20.- Continued.

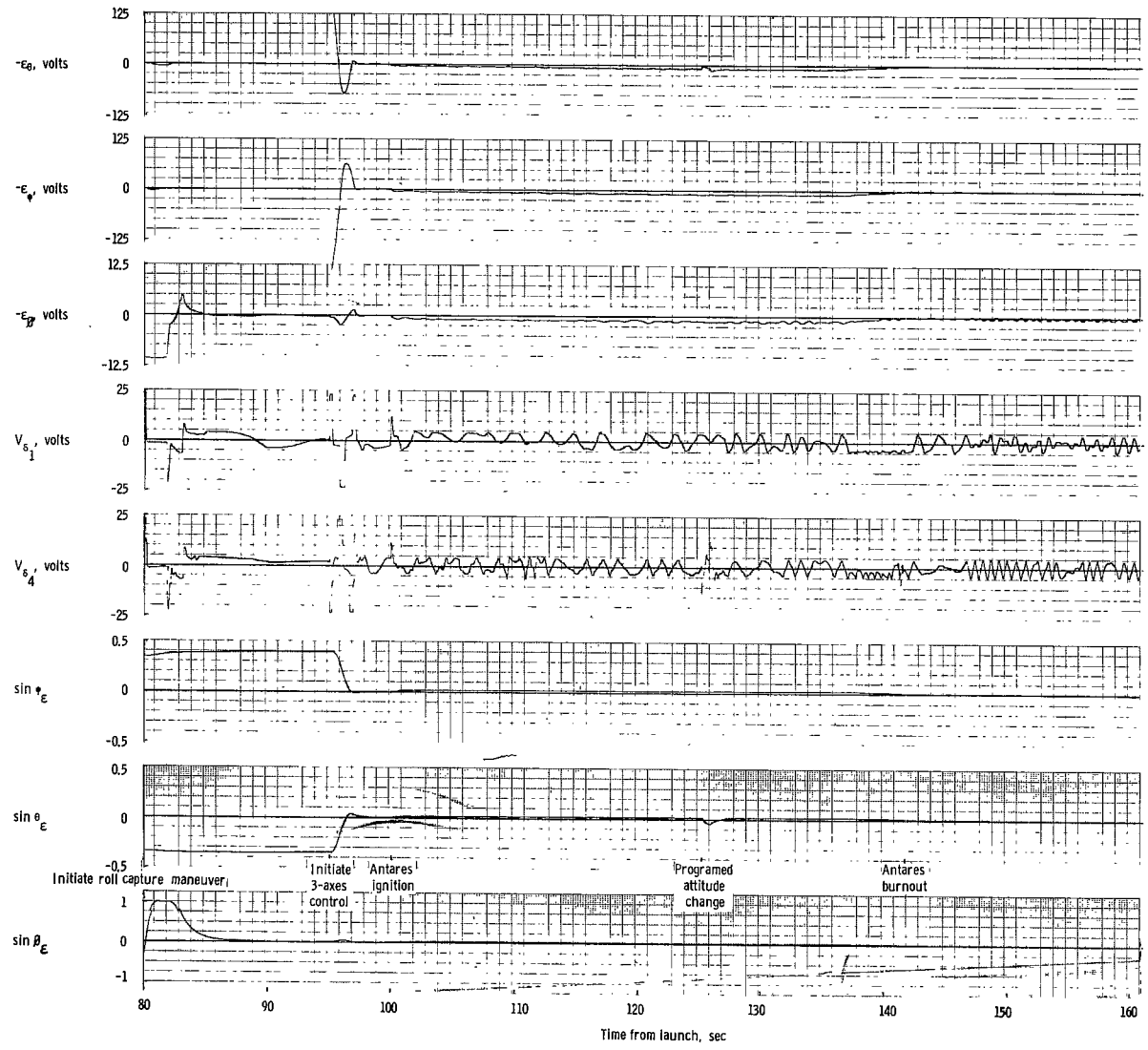

(c) Variation of $-\epsilon_\theta, -\epsilon_\psi, -\epsilon_\phi$, V_{δ_1}, V_{δ_4}, sin ψ_ϵ, sin θ_ϵ, and sin ϕ_ϵ with time.

Figure 20.- Continued.

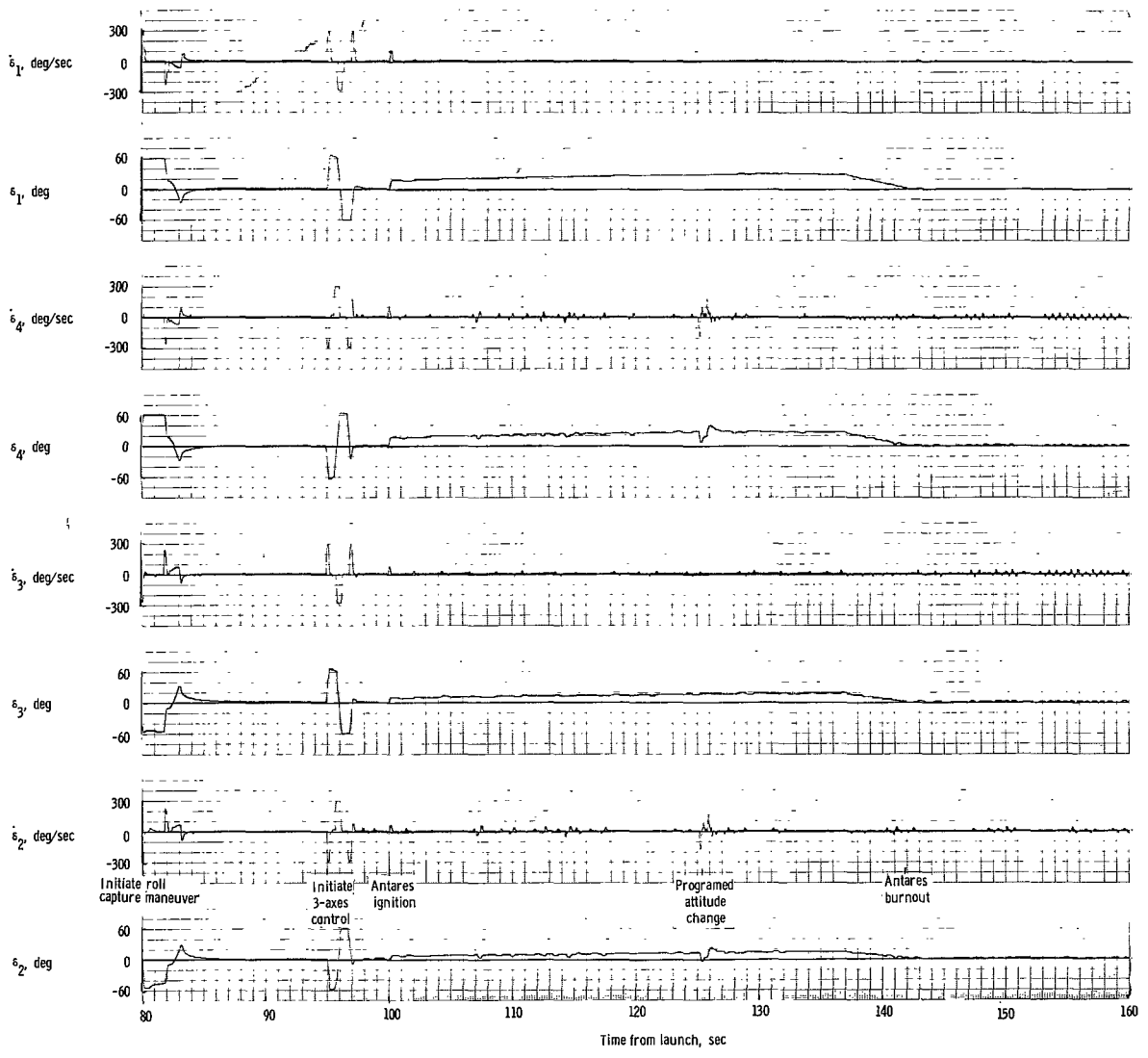

(d) Variation of $\dot{\delta}_1$, δ_1, $\dot{\delta}_2$, δ_2, $\dot{\delta}_3$, δ_3, $\dot{\delta}_4$, and δ_4 with time.

Figure 20.- Concluded.

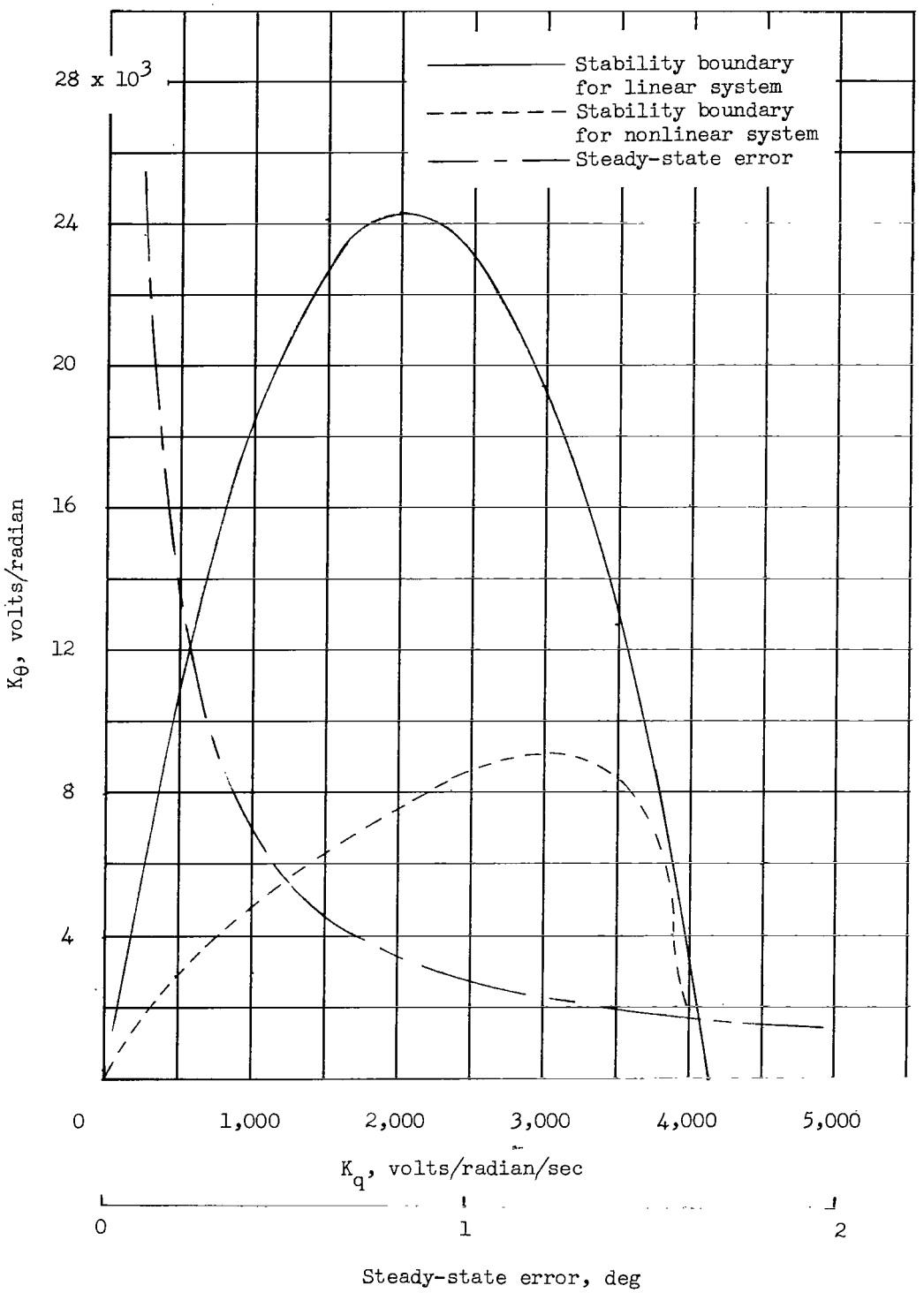

Figure 21.- Stability and steady-state error in pitch.

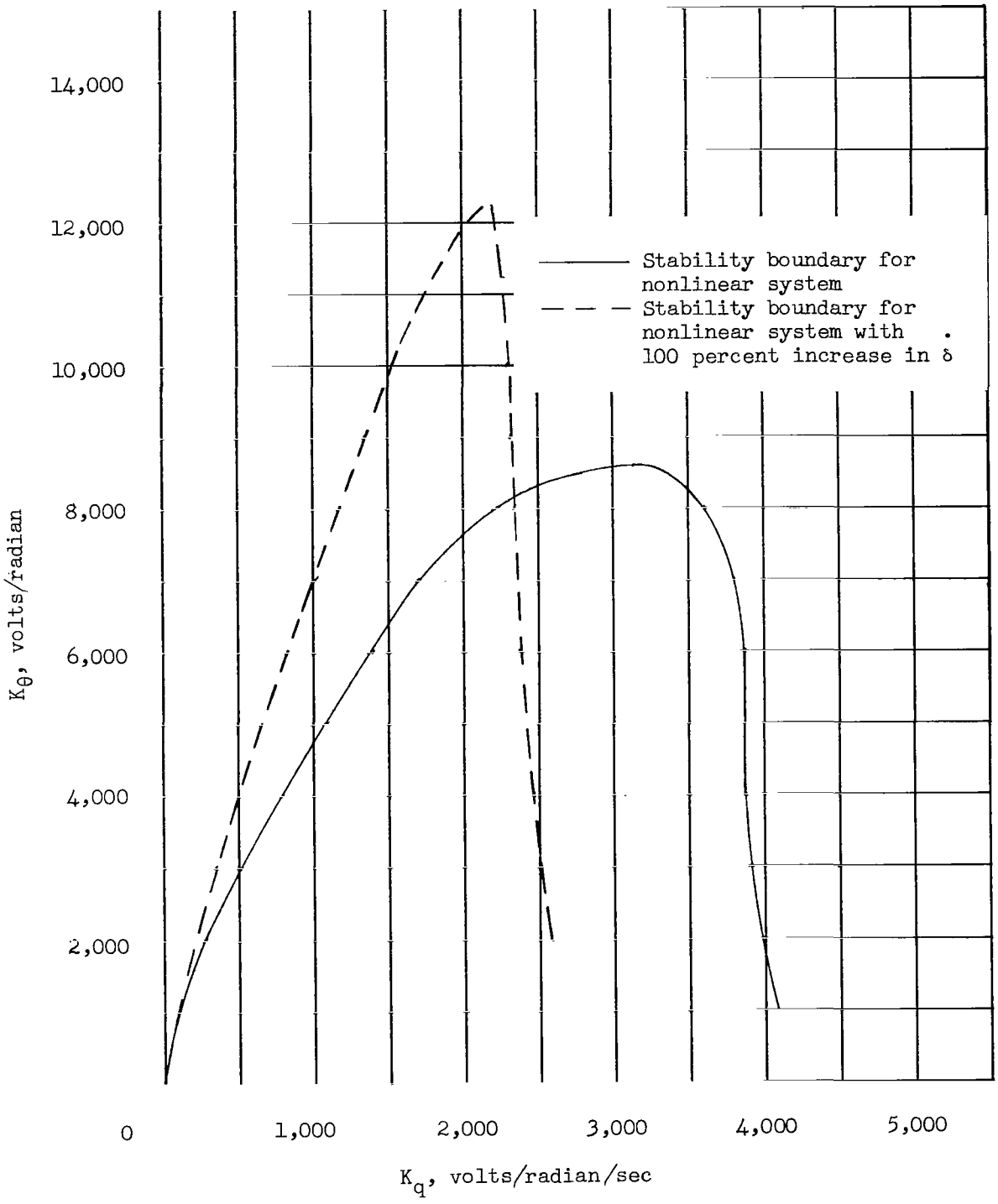

Figure 22.- Effect of control-rocket deflection rate on stability boundary in pitch.

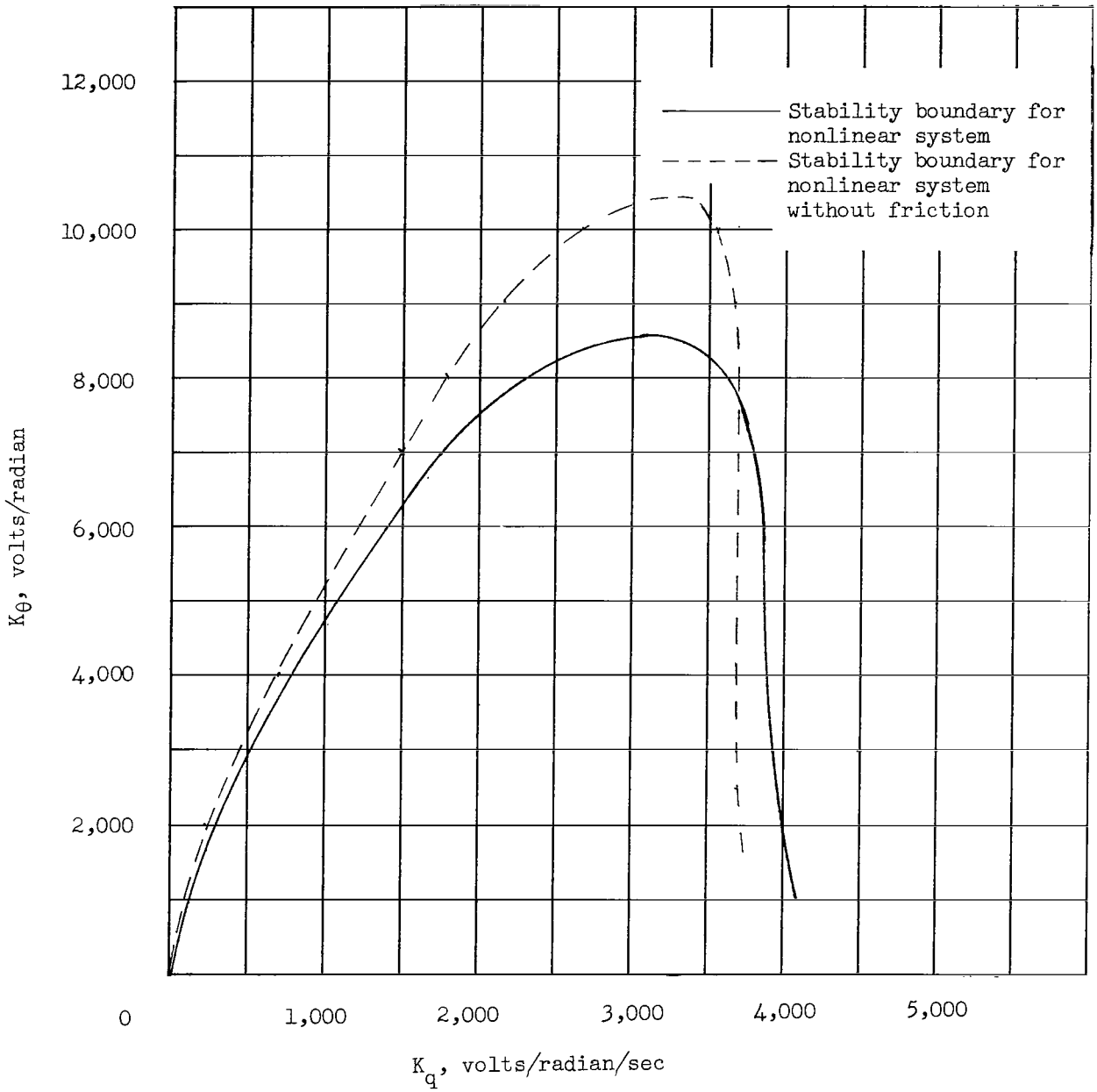

Figure 23.- Effect of control subsystem friction on stability boundary in pitch.

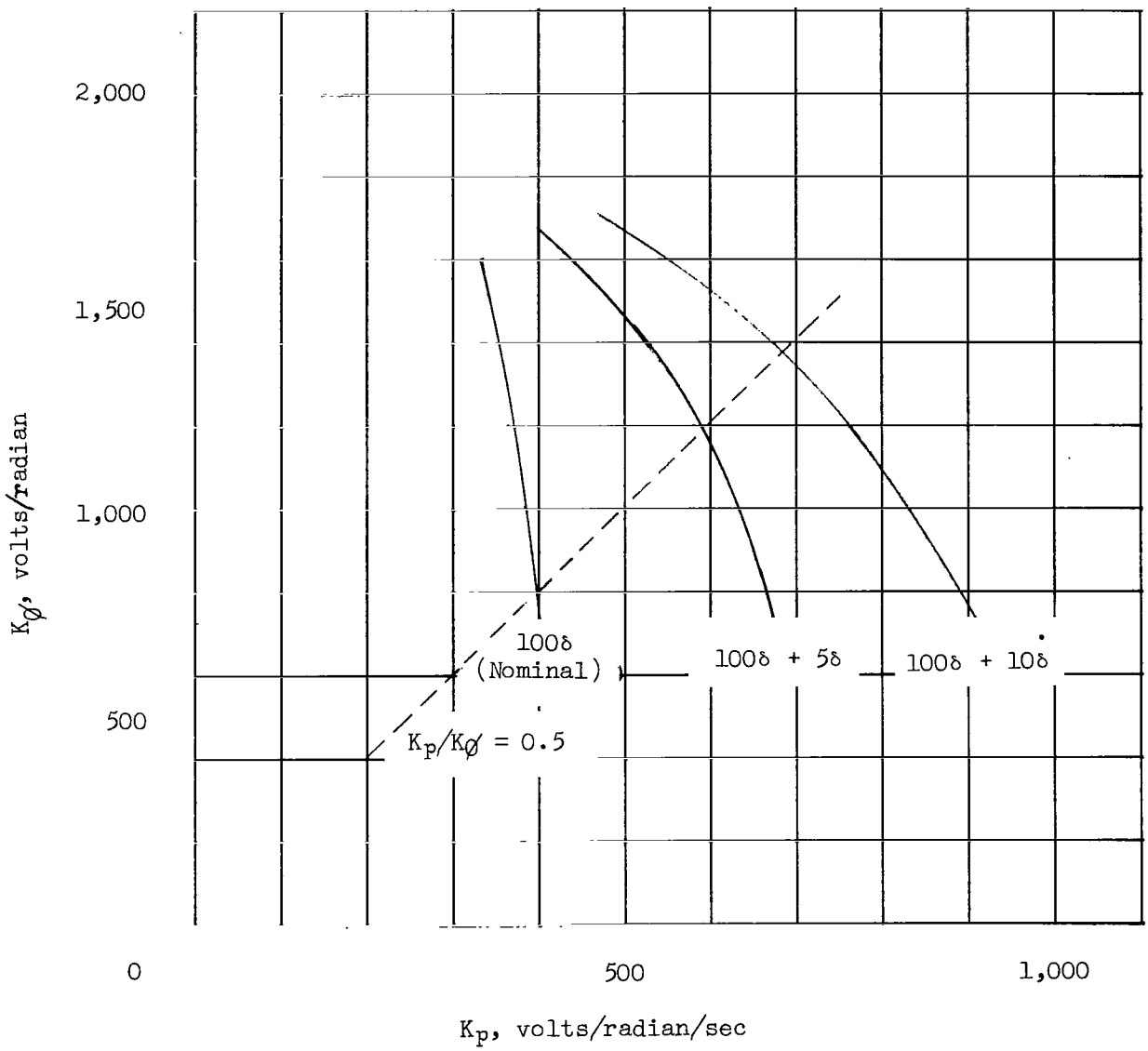

Figure 24.- Effect of control-rocket deflection rate feedback on nominal roll stability boundary.

"The aeronautical and space activities of the United States shall be conducted so as to contribute . . . to the expansion of human knowledge of phenomena in the atmosphere and space. The Administration shall provide for the widest practicable and appropriate dissemination of information concerning its activities and the results thereof."

—NATIONAL AERONAUTICS AND SPACE ACT OF 1958

NASA SCIENTIFIC AND TECHNICAL PUBLICATIONS

TECHNICAL REPORTS: Scientific and technical information considered important, complete, and a lasting contribution to existing knowledge.

TECHNICAL NOTES: Information less broad in scope but nevertheless of importance as a contribution to existing knowledge.

TECHNICAL MEMORANDUMS: Information receiving limited distribution because of preliminary data, security classification, or other reasons.

CONTRACTOR REPORTS: Technical information generated in connection with a NASA contract or grant and released under NASA auspices.

TECHNICAL TRANSLATIONS: Information published in a foreign language considered to merit NASA distribution in English.

TECHNICAL REPRINTS: Information derived from NASA activities and initially published in the form of journal articles.

SPECIAL PUBLICATIONS: Information derived from or of value to NASA activities but not necessarily reporting the results of individual NASA-programmed scientific efforts. Publications include conference proceedings, monographs, data compilations, handbooks, sourcebooks, and special bibliographies.

Details on the availability of these publications may be obtained from:

SCIENTIFIC AND TECHNICAL INFORMATION DIVISION

NATIONAL AERONAUTICS AND SPACE ADMINISTRATION

Washington, D.C. 20546